ABSTRACT

Title of Thesis:	STORMWATER QUALITY IMPROVEMENT BY AN ALUMINUM-BASED WATER TREATMENT RESIDUAL-INCORPORATED HIGH FLOW MEDIA PLUNGE POOL
	Guangyi Wang, Master of Science, 2020
Thesis Directed By:	Professor Allen P. Davis, Department of Civil and Environmental Engineering

Water treatment residual (WTR) is byproduct from the drinking water treatment process; WTR is made of aluminum-based or iron-based chemicals. It has been demonstrated as an advanced material to enhance phosphorus removal from stormwater runoff. In this field study, an aluminum-based WTR-incorporated high flow media (HFM) plunge pool in a residential area was monitored for 14 months to evaluate the removal of total suspended solids (TSS), phosphorus, and nitrogen in stormwater. Results indicate satisfactory removal of TSS, achieved via sedimentation and filtration. Moreover, total phosphorus (TP) concentrations were significantly reduced after treatment. All paired-sample events (13 events) exhibited positive (i.e., effluent EMC < influent EMC) TP removal. However, total nitrogen (TN) was not removed successfully due to $NO_3^- - N$ export through mineralization and nitrification processes. Dissolved aluminum leaching is less than 0.05 mg/L. An unexpected effluent seepage with high iron concentrations caused a “baseflow” in the downstream pipe, which was a significant challenge in this project.

STORMWATER QUALITY IMPROVEMENT BY AN ALUMINUM-BASED WATER TREATMENT RESIDUAL-INCORPORATED HIGH FLOW MEDIA PLUNGE POOL

by

Guangyi Wang

Thesis submitted to the Faculty of the Graduate School of the
University of Maryland, College Park, in partial fulfillment
of the requirements for the degree of
Master of Science
2020

Advisory Committee:
Professor Allen P. Davis, Chair
Associate Professor Birthe Veno Kjellerup
Assistant Professor Guangbin Li

Acknowledgements

This project was supported by the Low Impact Development Center, Inc., Prince George's County Department of the Environment (DoE), the Clean Water Partnership, and the National Fish and Wildlife Foundation Chesapeake Bay Stewardship Fund.

Table of Contents

List of Tables

List of Figures

List of Abbreviations

BMP: best management practice

DOP: dissolved organic phosphorus

DP: dissolved phosphorus

HFM: high flow media

PP: particulate phosphorus

SCM: stormwater control measurement

SRP: soluble reactive phosphorus

TN: total nitrogen

TP: total phosphorus

TSS: total suspended solids

WTR: water treatment residual

Chapter 1: Introduction

Stormwater runoff is been a major cause of environmental degradation in many surface waters as the urbanization process leads to fewer plants and less pervious surface, which allows little or no infiltration. Nutrients, primarily phosphorus and nitrogen, come from fertilizers, detergents, human and pet wastes, living and decaying plants, automobile exhausts, and atmospheric deposition, can be washed by stormwater into water bodies through surface runoff (USEPA 1999). Excessive nutrients input to receiving water bodies causes adverse aesthetic and biological impacts to the environment, the most common and one of most concern is eutrophication. Eutrophication is characterized by high density of algae and extensive mats of floating organisms owing to the excessive phosphorus and nitrogen enrichment needed for photosynthesis, resulting in degradation of water quality and reduction of biodiversity. Therefore, it is essential to implement some appropriate and effective solutions to manage stormwater and minimize the pollutant loads entering water bodies.

Various best management practices (BMPs), also known as stormwater control measurements (SCMs) have been widely implemented in urban areas to manage stormwater volume and mitigate the pollutants in stormwater. Bioretention and sand filters are common SCMs, which have been broadly applied and approved as technologies to effectively improve water quality in developed landscapes. Traditional bioretention and sand filters are very successful in particulate species removal, relying on physical removal mechanisms, especially sedimentation (i.e., particle settling) and filtration. Many SCM studies (Urbonas 1999; Hunt et al. 2008;

Li and Davis 2009; Barret 2010; Landsman and Davis 2018) reported excellent performance to remove total suspended solids (TSS) and particulate-bound pollutants like particulate phosphorus (PP) in the systems. However, traditional SCMs are less successful at capturing dissolved phosphorus (DP), which is defined as the amount of phosphorus that passes through a 0.45 μm filter (APHA/AWWA/WEF 1998), because chemical sorption/precipitation or biological processes are needed for DP immobilization. Phosphorus partitioning between particulate and dissolved phases is variable based on specific site conditions, therefore it is important to take both PP and DP removals into consideration for the SCM designs to reach an optimum overall phosphorus treatment effectiveness. Some SCM studies (Davis and Shokouhian 2006; Hatt et. al 2007; Cho et. al 2009; Brown 2013) reported that nitrogen removal is highly variable and generally poor because of the biogeochemical complexity of nitrogen species and various removal mechanisms including sedimentation/filtration, adsorption, mineralization, and biological transformations interacts in the SCMs. To improve dissolved pollutants removal, advanced technology needs to be developed as a replacement or update of the traditional SCMs.

Water treatment residuals (WTRs), sometimes called hydrosolids, are byproducts from the water treatment process in drinking water treatment facilities. They are made of non-toxic aluminum-based or iron-based chemicals, which have been demonstrated as novel supplement materials to mitigate phosphorus leaching and greatly enhance phosphorus removal from stormwater runoff. WTR offers a much greater phosphorus adsorption capacity than bioretention soil by the large specific surface area and abundant porous structure, which means more adsorption

sites available for phosphorus attachment. Adsorption occurs at oxide/hydroxide aluminum and iron interfaces; phosphate replaces hydroxyl (OH-) groups or water molecules (H_2O) and then reorganizes into a very stable binuclear bridge through mono ligand and/or bidentate ligand exchange mechanisms (Bohn et. al 1985). Some pilot and laboratory studies (Lucas et al. 2011; O'Neill and Davis 2012, Qiu et al. 2019) have demonstrated that WTR incorporated bioretention systems significantly increased phosphorus removal compared with traditional bioretention. However, as a fairly new technology, field performance of WTR incorporated SCMs on stormwater runoff treatment is sparse.

In this study, a WTR-incorporated high flow media (HFM) plunge pool was applied as a SCM to manage the stormwater runoff from a residential community with a 2.9 ha overall drainage area in Maryland, USA. The pollutants in this site are expected to be similar with most of residential areas, such as road dust, leaf decomposition and other wastes. The system was designed to collect the stormwater runoff and remove the pollutants washed by the runoff from the whole drainage area, instead of allowing it to discharge to the downstream creek directly. A 0.31 m HFM layer is the main functional part of the plunge pool, which was made by 10% WTR (by volume) and sand mixture. In order to systematically evaluate the water quality performance of the plunge pool, common stormwater pollutants including TSS, phosphorus, nitrogen and heavy metals were monitored during natural stormwater events from February 2019 to March 2020. The following objectives are identified to achieve the aim:

1. Evaluate the effectiveness of a WTR-incorporated HFM plunge pool for TSS, phosphorus, nitrogen, zinc, and copper removal, with the hypothesis that the SCM will perform well in TSS, phosphorus, and metals removal, but less efficient in nitrogen removal.
2. Detect whether Al leaching from the HFM, with the hypothesis that Al leaching will not be detected in the pH range typical of urban stormwater (Ostrom and Davis 2019).
3. Compare water quality results with other SCM studies, with the hypothesis that phosphorus removal is as effective as other WTR-incorporated SCMs, but more efficient than the traditional SCMs (without WTR applied).

Chapter 2: Methodology

Site Description

The experimental site is located at the intersection of Davis Avenue, Fort Drive, and Crosier Street, Suitland (Prince George's County), Maryland, USA (Figure 1 and Figure 2). A WTR-incorporated HFM plunge pool was constructed to manage the stormwater runoff from the residential community with a 2.9 ha overall drainage area. The construction work started in October 2018 and finished in December 2018. Figure 3 shows the experimental site before/during and after construction.

Figure 1. Experimental site location includes latitude and longitude (Google maps).

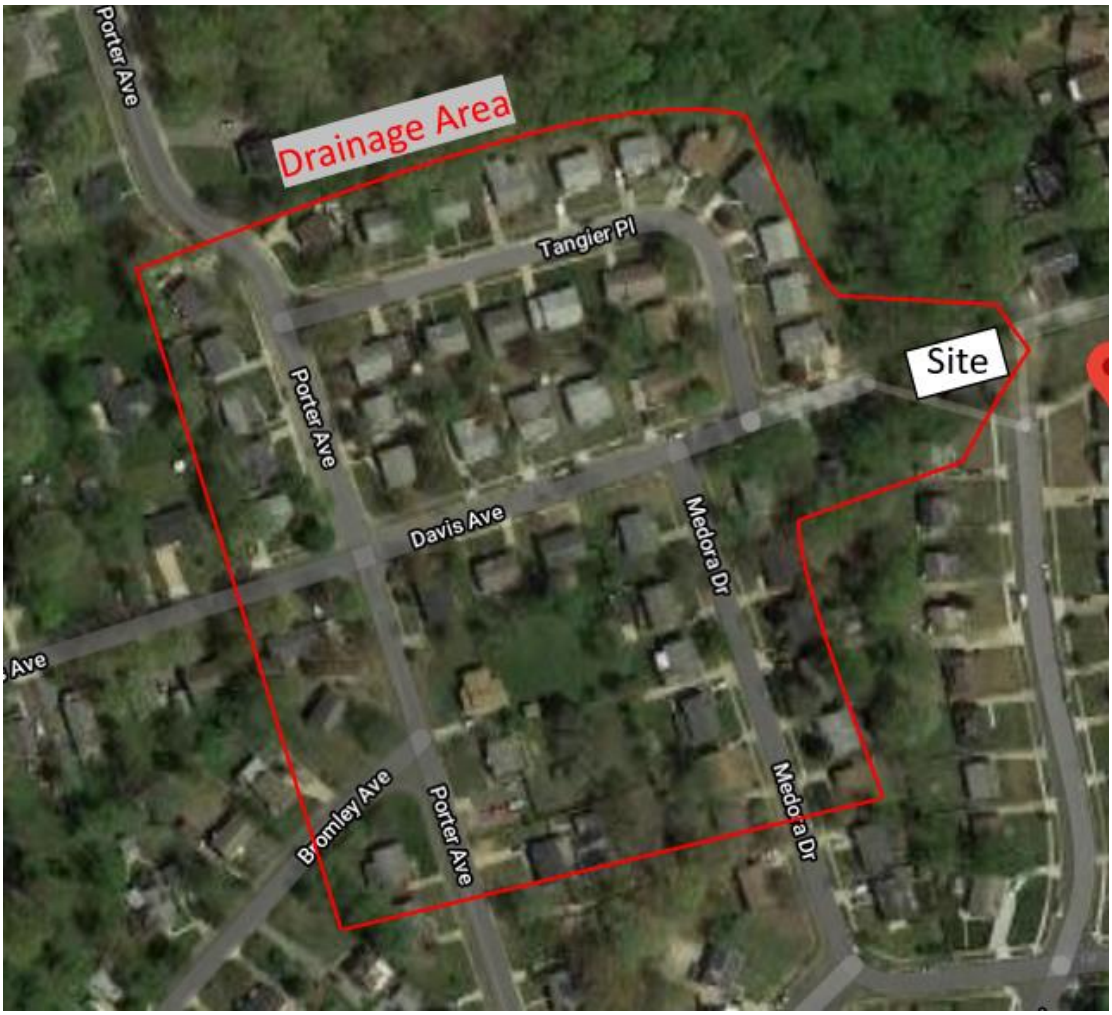

Figure 2. The overall drainage area and zoomed in experimental site location (Google maps).

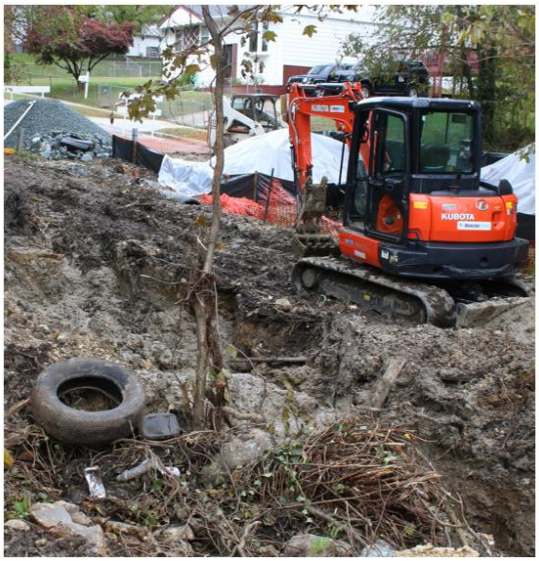

Figure 3. Photos of the experimental site a) before/during construction, and b) after construction was finished.

As Figure 4 shows, the plunge pool is located below a 0.38 m diameter inflow concrete pipe which collects the runoff from the drainage area. The plunge pool is nearly rectangular in shape (length=2 m, width=1.5 m), about 1 m in depth, with the volume about 3 m^3. The stormwater is treated by infiltrating through the 0.31 m HFM, which is the main functional part of the plunge pool. The HFM was made of 10% WTR (by volume) and Washed ASTM C-33 Fine Aggregate Concrete Sand mixture. The particle size distribution was summarized in Table 1. The sand is silica-based, which is often utilized for stormwater management applications. The WTR applied in this project is a clay-like material, which was obtained from the Dalecarlia Water Treatment Plant in Washington DC. Ostrom and Davis (2019), who used WTR from the same water treatment plant as our study, reported the aluminum content is 10,700 $\pm$ 1500 mg Al/kg dry sample in the WTR, and iron content is 925 $\pm$ 213 mg Fe/kg dry sample.

Table 1. Summary of particle size distribution of ASTM C-33 Fine Aggregate.

Sieve Size	Percent Pasing by Weight
3/8 in. (9.5 mm)	100
No. 4 (4.75 mm)	95 to 100
No. 8 (2.36 mm)	80 to 100
No. 16 (1.18 mm)	50 to 85
No. 30 (600 µm)	25 to 60
No. 50 (300 µm)	10 to 30
No. 100 (150 µm)	2 to 10

Note: Data are retrieved from: http://www.buildingresearch.com.np/index.php

After treatment, stormwater flows through a 0.15 m diameter PVC subsurface pipe system (Figure 5) to downstream creek. If the runoff inflow rate is greater than the infiltration rate during a relatively heavy rainfall, the plunge pool can retain runoff. When the plunge pool reaches to the maximum holding capacity, excess runoff can flow to the riprap outlet (flood control). The inflow and outflow pipe were set as the influent and effluent water quality samples collection points. The site was studied for 14 months, beginning February 2019.

Figure 4. The 0.38 m diameter inflow concrete pipe and the plunge pool (during a rainfall event).

Figure 5. 0.15 m diameter outflow PVC pipe.

Monitoring and Sampling Methodology

Water quality and hydrology were monitored at the experimental site during natural storm events from February 2019 to March 2020. Two ISCO 6712 Automated Portable Samplers (Teledyne ISCO, Lincoln, Nebraska) with integrated bubbler flow meters (ISCO 730 Bubbler Flow Module) were assigned at the upstream and downstream for influent and effluent stormwater quality samples collection and hydrology data monitoring. An ISCO (Lincoln, Nebraska) tipping bucket rain gauge (ISCO 674 Rain Gauge) with 0.254 mm discrete sampling was connected to the upstream autosampler to measure the precipitation depths. Bubbler tubes were connected to the autosamplers (flowmeters) and to the 0.38 m and 0.15 m Thel-Mar volumetric weirs installed in upstream and downstream pipes for measuring the water depths. Water depths were converted to flowrates by the autosamplers. Two 9.4-liter poly bottles were used to collect composite inflow and outflow stormwater samples. Sampling containers were cleaned with phosphorus-free detergent, acid-washed,

thoroughly rinsed with de-ionized water, and completely dried before using in the field.

Rainfall data from Weather Underground (https://www.wunderground.com/) was used to estimate the incoming precipitation depths. With the precipitation data, the inflow volumes were estimated using NRCS method (NRCS 1986):

$$S = \frac{2540}{CN} - 25.4 \quad Eq.1$$

$$I_a = 0.2 * S \quad Eq.2$$

$$Q_i = \frac{(P_i - I_a)^2}{(P_i - I_a) + S} \quad Eq.3$$

$$V_{Influent} = \frac{Q_i}{100} * A \quad Eq.4$$

$$The\ program\ was\ set\ as: "SAMPLE\ VOLUME: 10\ mL\ FOR\ EVERY\_\_\_\ L"$$

$$\frac{10\ mL}{\_\_\_\ L} = \frac{Expected\ Sample\ Volume}{Total\ Runoff\ Volume} = \frac{9.4\ L}{V_{Influent}} \quad Eq.5$$

where CN is the dimensionless curve number, given as 87 for this experimental site (from the project design plan); I_a is the initial abstraction (cm); S is the maximum potential retention of water by site soil (cm); Q_i is runoff depth (cm); P_i is the predicted individual storm depth (cm); $V_{Influent}$ is the predicted influent volume (m^3); and A is the overall drainage area, given as 28,975 m^2 (7.16 acres) for the experimental site (from the project design plan). This method works as a guidance to setup the programs. Autosampler programs were updated and revised one day before the expected rainfall events to make sure appropriate amounts of samples can be collected.

When the water depths in the pipes reached to enable levels, the autosamplers were activated. For upstream, when the water depth reached 0.005 m, the program was triggered; for downstream, 0.02 ~ 0.03 m was set as the enable level according to the baseflow level in the downstream pipe (the baseflow will be discussed in the following **Effluent Seepage Issue** section). Composite sampling was employed for both inflow and outflow. The programs were set as volume-weighted flow based, which means the samples concentrations were equal to the event mean concentrations (EMCs, will be defined in **Data Handling and Statistical Analyses** section).

Ice was added around the 9.2 L containers to keep the sample cool one day before summer rainfall events. After the rainfall stopped, the samples were picked up within 24 hours from the site, ice covered, and stored in an insulated box. Then they were transferred to University of Maryland Environmental Engineering Lab for analysis.

The water quality samples storage, preservation, and holding time strictly followed USEPA 1978 criteria. Samples for phosphorus and nitrogen analysis were acidified with 2 mL of concentrated sulfuric acid (Fisher Chemical) per liter of sample; samples for total recoverable metals analysis were acidified with 3 mL of 1:1 trace metal grade nitric acid (Fisher Chemical) per liter of sample; samples for dissolved elements were filtered through 0.22 μm membrane filters (Fisher Scientific) first then acidified. All sample bottles were sealed, labeled, and then frozen (< -25 °C) before testing. Parameters such as TSS and pH were tested immediately when samples were collected. Other parameters were analyzed before the maximum

holding time (up to 28 days for phosphorus and nitrogen; up to six months for metals).

Analytical Methodology

Water quality parameters measured included pH, TSS, total phosphorus (TP), DP, soluble reactive phosphorus (SRP, considered equal to dissolved phosphate), total nitrogen (TN), nitrate ($NO_3^- - N$), nitrite ($NO_2^- - N$), ammonium ($NH_4^+ - N$), total metals and dissolved metals include Al(III), Fe(III), Cu(II) and Zn(II) were analyzed using Standard Methods (APHA et al. 2012). Particulate phosphorus was calculated by subtracting DP from TP (PP = TP - DP). Dissolved organic phosphorus was calculated by subtracting SRP from DP (DOP = DP - SRP).

Sample pH, conductance and TSS were measured immediately when the samples were transferred to the lab. Sample pH and conductance were measured with a glass electrode pH/Ion/°*C* meter (Metter Toledo MA235, Greifensee, Swizerland). TSS was measured gravimetrically by Standard Method 2540 D.

TP was analyzed using potassium persulfate digestion (Standard Method 4500-P B.5) and colorimetric determination by the automatic ascorbic acid reduction method (Standard Method 4500-P F) at 880 nm using an AQ300 discrete analyzer (SEAL Analytical). DP and SRP samples were first filtered through 0.22 μm membrane filters (Fisher Scientific), then analyzed using methods identical to TP analysis, except without the digestion process for SRP. All phosphorus forms are reported as mg/L as P. The detection limit for TP, DP, SRP is 0.002 mg/L as P.

TN was measured using Standard Method 4500-N C with a Total Organic Carbon Analyzer with a Total Nitrogen Measuring Unit (TOC analyzer, Shimazdu, Kyoto, Japan). Stir bars were put into the TN vials to make sure the samples were well mixed during the analysis; the detection limit is 0.05 mg/L as N. $NO_3^- - N$ was measured using Standard Method 4500-NO_3^- and 4110 B and ion chromatography (ICS-1100, Dionex, Sunnyvale, CA). 4.5 mM Na_2CO_3/1.4 mM $NaHCO_3$ eluent solution was run isocratically through an anion-exchange column with 150 mm length, 4 mm ID, and 6.5 mm polymer particle size (IonPac AS22 Fast IC column, Dionex, Sunnyvale, CA) at a flow rate of 1.2 mL/min (Ostrom and Davis 2019). The detection limit is 0.1 mg/L as N. $NO_2^- - N$ was measured spectrophotometrically in an AQ300 discrete analyzer at 520 nm following Standard Method 4500-NO_2^-. The detection limit is 0.0006 mg/L as N. $NH_4^+ - N$ was measured photometrically in an AQ300 discrete analyzer at 660 nm following Standard Method 4500-NH_3 H and 4500-NH_3 G. The detection limit is 0.003 mg/L as N. All nitrogen forms are reported as mg/L as N.

Stormwater samples were digested with 1:1 trace metal grade nitric acid (Fisher Chemical) and 1:1 trace metal grade hydrochloric acid (Fisher Chemical) following by EPA Method 200.8 before measuring total Al(III), Fe(III), Cu(II) and Zn(II) concentrations. For dissolved metals, an appropriate volume of 1:1 trace metal grade nitric acid (Fisher Chemical) was added to adjust the acid concentration of the aliquot to approximate a 1% (v/v) nitric acid solution. Total and dissolved metals concentrations were measured using inductively coupled plasma atomic emission spectroscopy (ICP-AES) (ICPE-9000 Plasma Atomic Emission Spectrometer,

Shimazdu, Kyoto, Japan). The detection limit for Al(III) and Fe(III) is 25 μg/L, and it is 10 μg/L for Cu(II) and Zn(II).

All laboratory analytical procedures were calibrated every time before they were used. The standards solutions with different ranges were used based on the stormwater samples concentrations and linear calibrations of standard curves had no less than 0.999 correlation coefficients. Additionally, all samples were measured in triplicate, in which the variation of the three measurements did not exceed 10%. If a concentration was below the detection limit, a value equal to 1/2 of the detection limit was used for statistical purposes.

Data Handling and Statistical Analyses

Discrete rainfall events were identified if separated by a dry period greater than 12 hours. Runoff volumes (V) were determined by numerically integrating the flowrate over time:

$$V = \int_{t_1}^{t_2} Q(t) * dt \qquad Eq. 6$$

which equals the area under the hydrograph. Since there is always a baseflow contributing to the outflow, the outflow hydrograph area is not the true outflow volume. To determine the true value, outflow volume was calculated by subtracting the baseflow volume from the total volume. (baseflow will be discussed in the **Effluent Seepage Issue** section). The Event Mean Concentration (EMC) was used to represent the volume-weighted pollutant concentration throughout an entire storm event:

$$EMC = \frac{\int_{t_1}^{t_2} Q(t) * C(t) * dt}{\int_{t_1}^{t_2} Q(t) * dt} \qquad Eq.7$$

which is the mean concentration from triplicate measurements. Q(t) is the runoff flowrate at time t; t_1 is the time when rainfall starts and t_2 is the time when rainfall ends; C(t) is the concentration collected at time t. Overall cumulative input/output pollutant mass (M) was calculated by:

$$M = EMC * V \qquad Eq.8$$

Overall volume-weighted average (mean) EMCs were calculated by cumulative mass divided by the cumulative volume for all collected samples:

$$Overal\ Volume - Weighted\ Average\ EMC = \frac{\sum_{i=1}^{n} M_i}{\sum_{i=1}^{n} V_i} \qquad Eq.9$$

the overall volume-weighted average EMC discussed in the following sections are from paired-sample events (the events have both influent and effluent water quality samples and hydrology data) unless specifically noted.

Exceedance probability plots were used to present water quality data in order to emphasize the treatment outcome and evaluate the plunge pool performance. They were created by ranking the measured values from largest to smallest and plotted on a log scale, implying their log-normal distribution nature, as described by Li and Davis (2009). The Wilcoxon Signed-Rank Test was used to determine if the improvement in water quality were statically significant for paired data.

Chapter 3: Results and Discussion

Effluent Seepage Issue (Baseflow)

The presence of an effluent seepage was a significant challenge in this project. It was expected that no influent or effluent would occur during dry periods because of no rainfall. However, it was noticed that there was always an effluent flow from the downstream pipe even when the upstream pipe was totally dry during times of no rainfall. This indicates that a "baseflow" existed, which continuously contributed to the effluent. No leak could be detected since all pipelines are underneath the ground, so it was assumed that the downstream pipe was cracked somewhere.

A mass balance method was used to eliminate the effects of the baseflow to the effluent concentrations. Figure 6 describes the inflow, baseflow and outflow in detail. The inflow pipe collected the runoff from the drainage area. Then the runoff discharged from the inflow pipe into the plunge pool; $Q_{Influent}, C_{Influent}$ refer to the flowrate and concentration of runoff discharged from the inflow pipe. The runoff discharged into the plunge pool and was treated by passing through the HFM, then flowed into the outflow pipe. $Q_{Effluent}, C_{Effluent}$ refer to the flowrate and concentration of the runoff discharged from the HFM, where $C_{Effluent}$ is the true effluent concentration we are looking for. However, the baseflow flowed into the outflow pipe and mixed with the true effluent. $Q_{Baseflow}, C_{Baseflow}$ represent the flowrate and concentration of the baseflow. After mixing, the combined flow discharged from the outflow pipe and was collected. $Q_{Combined}, C_{Combined}$ represent the flowrate and concentration of the combined flow.

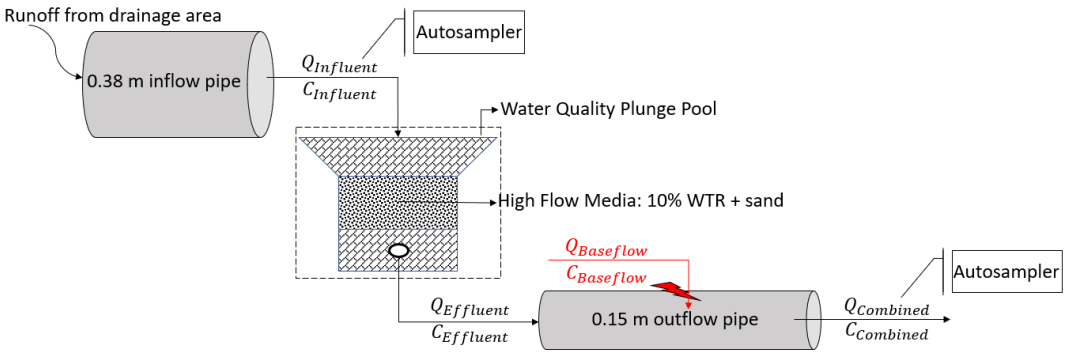

Figure 6. Flow description in the experimental site showing the impact of baseflow on the effluent.

According to the basic mass balance method:

$$C(EMC) = \frac{\sum_{i=0}^{n} V_i * C_i}{\sum_{i=0}^{n} V_i} \qquad Eq.10$$

the target concentration was calculated using:

$$C_{Combined} = \frac{C_{Effluent} * V_{Effluent} + C_{Baseflow} * V_{Baseflow}}{V_{Effluent} + V_{Baseflow}} \qquad Eq.11$$

$$V_{Combined} = V_{Effluent} + V_{Baseflow} \qquad Eq.12$$

$$C_{Effluent} = \frac{C_{Combined} * V_{Combined} - C_{Baseflow} * V_{Baseflow}}{V_{Combined} - V_{Baseflow}} \qquad Eq.13$$

where $C_{Effluent}$ is the target/true effluent concentration; $C_{Combined}$ is the measured concentration of the combined flow; $C_{Baseflow}$ is the measured concentration of baseflow (baseflows were collected one day before the rainfall events); $V_{Combined}$ is the combined/total effluent volume, determined from the autosampler output; $V_{Baseflow}$ is the baseflow volume, which is calculated using:

$$V_{Baseflow} = Q_{Baseflow} * t \qquad Eq.14$$

where $Q_{Baseflow}$ is the average baseflow flowrate; t is the runoff duration from the effluent hydrograph. An example of how the $V_{Combined}$ and $V_{Baseflow}$ were determined is presented in the **Appendix**.

Table 2. Summary of the characteristics of the baseflow; comparison among true effluent, baseflow and combined effluent EMCs (paired-samples only).

	Effluent EMC (Calculated, mg/L)		Baseflow EMC (mg/L)		Combined EMC (Measured, mg/L)	
Pollutant	Range	Median	Range	Median	Range	Median
TSS	<1 - 80	11	8 - 112	32	<1 - 107	17
TP	0.006 - 0.168	0.022	0.010 - 0.062	0.018	0.006 - 0.157	0.015
TN	0.259 - 4.040	0.832	0.350 - 0.840	0.577	0.329 - 3.714	0.645

Table 2 summaries the characteristic of the baseflow. Comparison was made among true effluent, baseflow and combined effluent EMCs to show how the baseflow affected the effluent concentrations. The baseflow has relatively low TP and TN concentrations. The baseflow and effluent have similar TP EMCs, whereas the median TN EMC of the baseflow is less than the effluent. The maximum effluent TP EMC is 1.7 times greater than the baseflow, and the maximum effluent TN EMC is 3.8 times greater than the baseflow. Based on the comparisons, TP concentrations in the baseflow are similar or less than in the effluent, and TN concentrations in the baseflow are less than the effluent. Therefore, the effluent TP and TN results may not be affected much by the baseflow because the TP and TN concentrations are relatively low concentrations in baseflow.

However, the TSS concentrations in baseflow are relatively high, which might affect the effluent results. As Table 2 shows, the minimum, maximum, and median values of TSS in the baseflow are higher than in the effluent. The median TSS EMC in the baseflow is 32 mg/L, which is 1.9 times greater than in the effluent. Comparing the median TSS EMC, the baseflow has the highest value, whereas effluent has the lowest. The combined flow is in-between since it was combined by the baseflow and effluent.

The baseflow shows extremely high concentrations of iron (digested samples), with a median EMC equal to 5 mg/L, and maximum EMC of 7 mg/L. (will be revised after measuring the rest of samples). The high iron concentrations were reflected visually in the baseflow samples. It was noticed that the well-mixed baseflow samples always had a brownish color. The color was caused by brownish particulate matter, which was easily detected after the samples settled. Furthermore, a similar color was detected in the effluent samples. Since the influent samples were generally clear, it was hypothesized that the brownish particles in the effluent are from the baseflow. Measurements showed high concentrations of iron in the combined effluent samples as well, which verified the hypothesis further (need to add data).

Figure 7 shows well-mixed stormwater samples of influent, effluent, and baseflow collected on October 10, 2019, which are representative of the general conditions for all stormwater samples. The influent samples were generally clear, with some suspended solids, large gravel particles or leaves. However, the baseflow samples, as well as the effluent samples, always had the brownish colors. As Figure 8 shows, sediments are present in each bottle, especially for the baseflow and effluent sample. The influent samples had the least amount of sediments, while baseflow samples had the most. Figure 9 shows remaining solids after filtering samples through 0.22 μm filters, which provides another view of the sediments in each sample. A relatively small amount of solids with black and grey color attached to the filter came from the inflow sample. Baseflow and effluent samples left solids with brownish color on the filters. The amount of solids in three samples had a sequence: inflow < outflow < baseflow. During the experiments, we frequently found more filter papers

were needed to filter same amount of baseflow samples, which suggests it has a high solids concentration.

Figure 7. Well mixed stormwater samples from the inflow, outflow and baseflow, collected October 10, 2019.

Figure 8. Settled stormwater samples from the inflow, outflow and baseflow, collected October 10, 2019.

Figure 9. Solids on the 0.22 µm filter: stormwater samples from the inflow, outflow and baseflow collected October 10, 2019.

There are two possible sources for the high iron concentrations in the baseflow; one is the iron leaching from the WTR, the other one is by groundwater intrusion. Simple mass balance calculations indicate that the most possible iron source is the groundwater instead of the WTR leaching.

The plung pool has been operational for over 1.5 years (about 550 days). The flowrate of the baseflow was constant during a single rainfall event, but varied with different events, ranging from 0.02-1.4 L/s. The iron concentrations in the baseflow ranged from 4143 to 7483 µg/L. With this data, the export mass of iron is ranged from 3,938 to 497,829 g (details shown in **Appendix**).

Ostrom and Davis (2019) used the same WTR and reported that the iron content is 10,900 mg Fe/kg in the air-dry WTR; the moisture contents are 3.2 g wet/g

dry for wet WTR. 10% wet WTR (by volume) was applied into the HFM, and the bulk density of WTR is 0.56 g/cm^3. The volume of the HFM is 0.51 cubic meters. With this information, the total mass of iron is approximately 311 g. Therefore, the smallest export mass of iron is 13 to 1600 times greater than the estimated total mass of iron in the WTR, which indicates that WTR is not the source of iron in the baseflow.

Characterization of Monitored Storm Events

From February 2019 to March 2020, 25 stormwater events were monitored. 22 influent and 15 effluent water quality samples were collected, in which 13 are paired-sample (have influent and effluent samples from a single event). TSS, TP, DP and SRP were analyzed for all collected samples. TN, $NO_3^- - N$, $NO_2^- - N$ and $NH_4^+ - N$ were analyzed for samples collected from the first half year. The precipitation depths, influent volumes, combined flow volumes, baseflow volumes, and effluent volumes are summarized in Table 2 for all collected stormwater quality events. Effluent volume was calculated using Eq.12.

Table 3. Summary of 25 monitored stormwater events at the WTR-incorporated HFM plunge pool experimental site.

Date	Precipitation (cm)	$V_{Influent}$ (m^3)	$V_{Combined}$ (m^3)	$V_{Baseflow}$ (m^3)	$V_{Effluent}$ (m^3)
March 31, 2019	0.08	0.54	0.31	0.29	0.02
April 8, 2019	0.10	0.97	0.33	0.18	0.15
April 13, 2019	0.76	17.78	1.43	1.30	0.13
April 15, 2019	0.61	15.76	4.20	3.56	0.63
June 9, 2019	1.14	238.92	21.39	11.52	9.87
June 17, 2019	0.33	39.09	25.72	21.60	4.12
June 18, 2019	0.33	42.33	12.64	10.80	1.84
July 2, 2019	1.07	52.05	-	-	-
July 4, 2019	0.61	134.58	34.70	15.84	18.86
August 13, 2020	0.18	36.12	37.97	18.00	19.97
October 13, 2019	0.99	262.20	-	-	-
October 26, 2020	0.53	12.54	15.54	1.58	13.95
November 18, 2019	0.58	185.54	-	-	-
November 22, 2019	0.94	173.83	-	-	-
November 23, 2019	1.47	76.10	82.76	60.48	22.28
December 1, 2019	1.40	113.28	20.48	7.92	12.56
December 13, 2019	1.09	22.14	13.16	4.86	8.30
December 16, 2019	0.48	9.88	10.16	2.59	7.57
December 17, 2019	0.53	2.25	9.90	6.30	3.60
February 4, 2020	0.13	4.47	3.44	2.92	0.53
February 10, 2020	2.18	24.10	22.75	2.88	19.87
February 12, 2020	0.94	0.18	15.84	6.48	9.36
March 13, 2020	0.56	18.69	-	-	-
March 14, 2020	0.43	15.63	-	-	-

Note: No effluent collected from July 2, 2019, October 13, 2019, November 18, 2019, November 22, 2019, March 13, 2020 and March 14, 2020 due to equipment issues.

Rainfall depths for the 25 collected stormwater events ranged from 0.08 to 2.18 cm. The distribution of events was compared with historical data for the state of Maryland (Kreeb 2003). The cumulative frequency of events more than 6.35 mm in the historical study is 47.5%, whereas it is about 50% in this study. This indicates that this study covers all types of stormwater events, with no bias towards to larger or smaller ones.

The ideal relationship between influent volumes and precipitation is predicted using the NRCS method (NRCS 1986) Eq. 1 to Eq. 4 and shown in Figure 10. The points in the figure represent all detected stormwater events. Most of the detected

stormwater events points are located above the NRCS Method curve, whereas several points are far away from the curve. Several reasons may cause the difference: 1). extra runoff coming from adjacent grass areas may cause the measured influent volume to be more than expected; 2). the given curve number and overall drainage area are estimated values, which may cause the difference; and 3). antecedent dry period and rain intensity may cause the difference (Doan and Davis 2017). To eliminate the bias, a new CN was determined to be 94 by trial and error to allow the most detected storm points to be located on the NRCS method curve and to have other points distributed uniformly on both sides of the curve (Figure 11). The new CN is greater than the given CN in the project design plan, which indicates the runoff potential in the site was underestimated, and the soil in the site is less permeable than estimated.

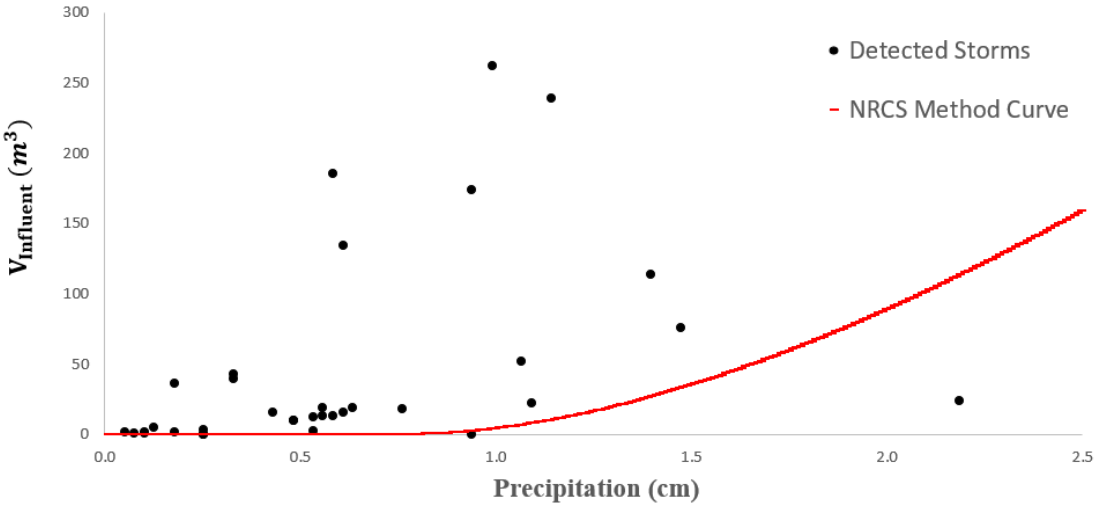

Figure 10. Stormwater volume from the watershed as a function of precipitation. The line is a prediction using the NRCS method (CN = 87).

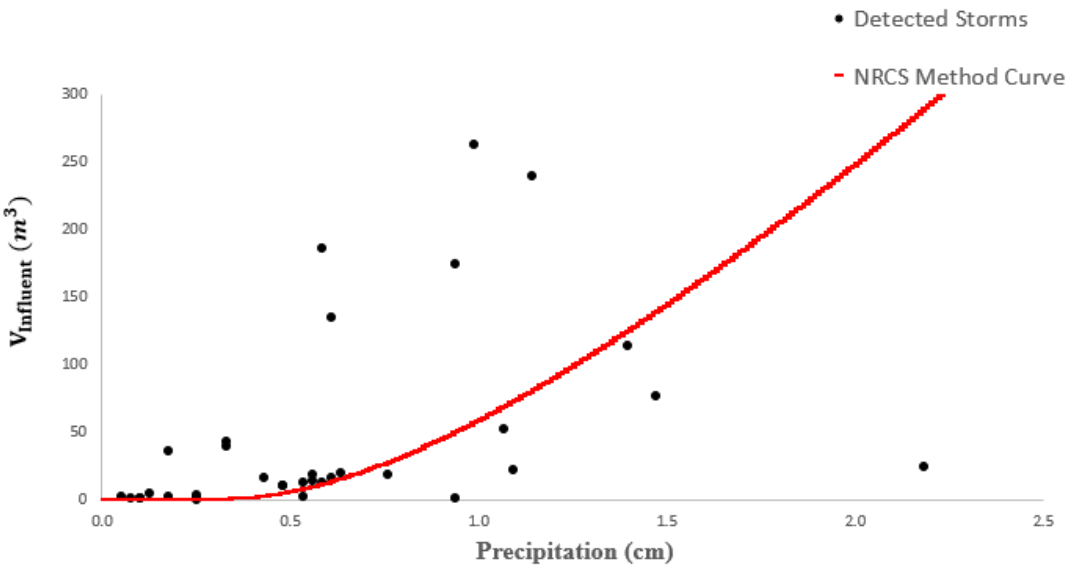

Figure 11. Stormwater volume from the watershed as a function of precipitation. The line is a prediction using the NRCS method (CN = 94).

Total Suspended Solids

The plunge pool had a good performance in TSS removal as other SMCs. The individual influent TSS EMCs ranged from 5 to 352 mg/L (median = 39 mg/L, 22 events), whereas individual effluent TSS EMCs ranged from < 1 to 80 mg/L (median = 13 mg/L, 15 events). The highest influent TSS EMC in this study is one order of magnitude lower than the result from the WTR retrofitted bioretention, 1274 mg/L, found by Liu and Davis (2013). Figure 12 shows the exceedance probability plot for the TSS influent and effluent. About 76% of the effluent EMCs met the 25 mg/L TSS water quality target value (Davis and McCuen 2005) compared to about 43% for the influent, which indicates effective TSS removal was achieved in the plunge pool.

Water quality results for all paired-sample studies are summarized in Table 3. Figure 13 shows the influent and effluent TSS EMCs for 13 paired-sample events. Ten of them showed positive TSS removal (i.e., effluent EMC < influent EMC). The

EMC removal efficiencies for those ten events ranged from 16.4% to 99.7% (median = 76.2%; 10 events). Three events exhibited negative TSS removal, which might be attributed to the iron particles from the baseflow. The Wilcoxon Signed-Rank Test determined that the effluent TSS was significantly reduced compared with the influent (p-value = 0.03318).

Table 4. Water quality performance data for the storm events monitored at the plunge pool.

		Influent EMC (mg/L)		Effluent EMC (mg/L)	
Pollutant	N (Number of Events)	Range	Mean (Median)	Range	Mean (Median)
TSS	13	5 - 352	50 (24)	<1 - 80	18 (11)
TP	13	0.035 - 0.396	0.160 (0.121)	0.006 - 0.168	0.042 (0.022)
PP	13	0.011 - 0.191	0.076 (0.071)	<0.002 - 0.093	0.014 (0.007)
DP	13	0.017 - 0.205	0.084 (0.056)	0.006 - 0.130	0.028 (0.013)
SRP	13	0.007 - 0.099	0.049 (0.031)	<0.002 - 0.051	0.014 (0.009)
DOP	13	<0.002 - 0.125	0.035 (0.025)	<0.002 - 0.079	0.014 (0.005)
TN	7	0.531 - 2.805	1.345 (1.310)	0.259 - 4.040	1.345 (0.832)
$NO_3^- - N$	7	<0.002 - 0.716	0.425 (0.197)	<0.002 - 2.314	0.568 (0.036)
$NO_2^- - N$	7	0.014 - 0.024	0.019 (0.021)	0.019 - 0.117	0.032 (0.021)
$NH_4^+ - N$	7	<0.002 - 0.268	0.112 (0.076)	<0.002 - 0.174	0.049 (0.017)

Note: The data in the table are from paired-sample events only.

The overall volume-weighted average influent TSS EMC is 50 mg/L, which is lower than results from other SCM studies, ranging from 65 to 140 mg/L (Li and Davis 2009; Liu and Davis 2013; Landsman and Davis 2018). He et al. (2010) concluded that the composition of solids on urban surfaces is highly dependent on location and land cover/land use. Irish et al. (1995) found that rainfall volume and intensity affect influent TSS concentrations as well. The overall volume-weighted average effluent TSS EMC is 18 mg/L, corresponding to a 63.9% EMC removal, which supports TSS removal was successful. Liu and Davis (2013) reported TSS were significantly removed in the WTR-retrofitted bioretention with the mean EMCs

reduced from 97 to 6 mg/L, and concluded that WTR did not harm the filtration mechanism in the bioretention media.

As discussed above, the iron particles from the baseflow impact the TSS export. However, using the mass balance method it appears that significant TSS reduction occurs.

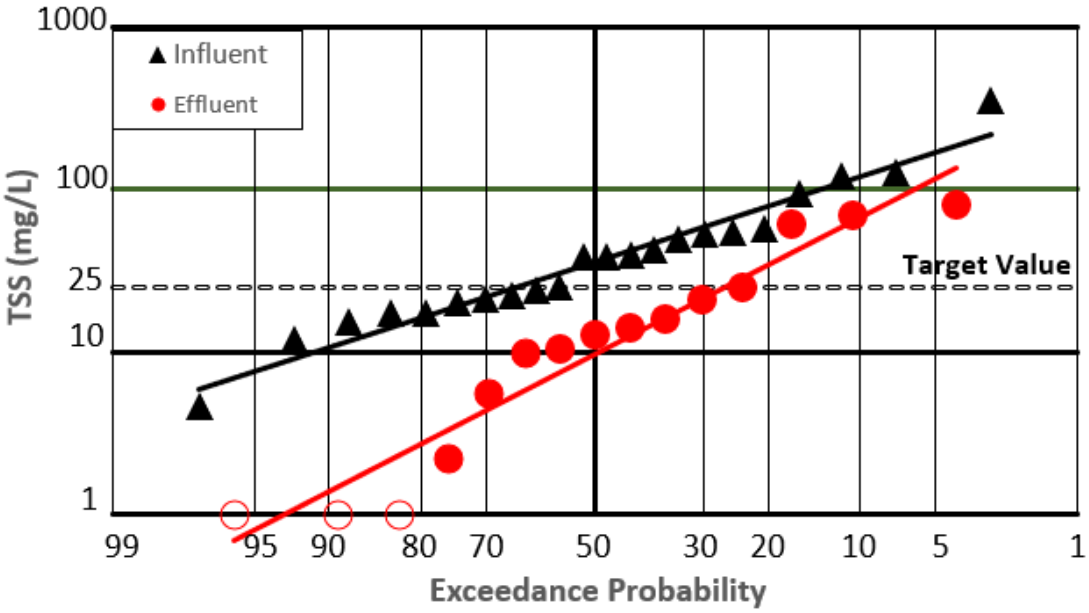

Figure 12. Exceedance probability plot of influent and effluent TSS EMCs. Values below the detection limit are plotted as one half of the detection limit and are shown as open symbols.

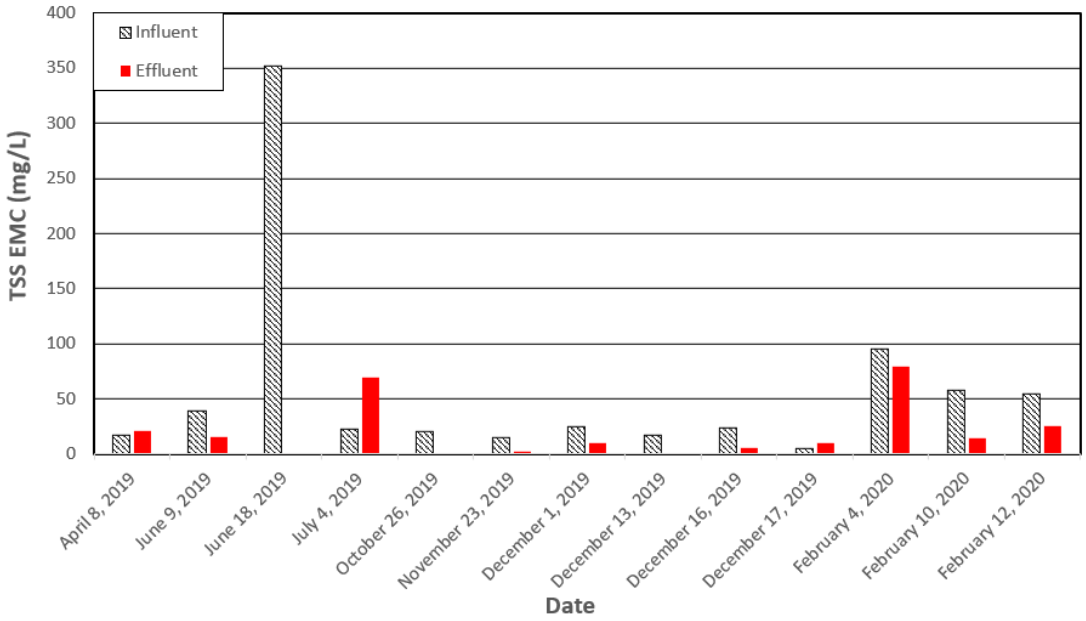

Figure 13. Influent and effluent TSS EMCs for 13 paired-sample events.

Phosphorus

Total Phosphorus

The plunge pool showed excellent performance for TP removal. The individual influent TP EMCs ranged from 0.026 to 0.74 mg/L (median = 0.16 mg/L; 22 events), whereas the individual effluent TP EMCs ranged from 0.006 to 0.17 mg/L (median = 0.024 mg/L; 15 events), respectively. In this study, the highest TP EMC was detected as 0.74 mg/L, which was measured from the influent samples collected on October 13, 2019. The suggested reason causing this was an extremely long dry period (over 7 weeks) before this rainfall event. Large amounts of leaves flushed into the plunge pool (Figure 14). The leftover dead leaves act as a nutrient source and may have contributed significantly to this high level (Brown et al. 2013; Shumilovskikh et al. 2015). Doan and Davis (2017) found a similar phenomenon, with a very high TP level of 1.67 mg/L in an event which had over two weeks since the previous rain.

Natarajan and Davis (2016) also reported the maximum phosphorus input might happen in the fall due to decomposition of leaves and grasses releasing nutrients. Figure 15 shows the exceedance probability plot for the influent and effluent TP EMCs. There is a clear difference in the data sets. The 10^{th} and 90^{th} percentile influent TP EMCs are 0.064 and 0.39 mg/L, respectively, whereas the 10^{th} and 90^{th} percentile effluent TP EMCs are 0.010 and 0.13 mg/L. About 70% of the effluent EMCs met the EPA recommended 0.03656 mg/L TP for rivers and streams in Ecoregion XIV (USEPA 2000), compared to only 7% for the influent, which supports an effective TP removal.

Figure 16 shows influent and effluent TP EMCs for 13 paired-sample events. All paired-sample events exhibited positive TP removal. The EMC removal efficiencies ranged from 36.3% to 92.4% (median = 83.8%; 13 events). There are two events with input TP EMCs greater than 0.3 mg/L. The maximum influent TP EMC is 0.4 mg/L for the paired-sample events. The corresponding effluent TP EMC was reduced to 0.17 mg/L after treatment, with a 57.5% removal. Another event had input TP EMC equal to 0.31 mg/L; after treatment, the effluent TP EMC was reduced to 0.045 mg/L, which corresponds to 85.7% EMC removal. These data indicate that the plunge pool performed well with a high TP input. The Wilcoxon Signed-Rank Test indicates that the difference between influent and effluent EMCs are statistically significant (p-value = 0.00148).

Figure 14. Leaves in the plunge pool. Photo taken October 14, 2019.

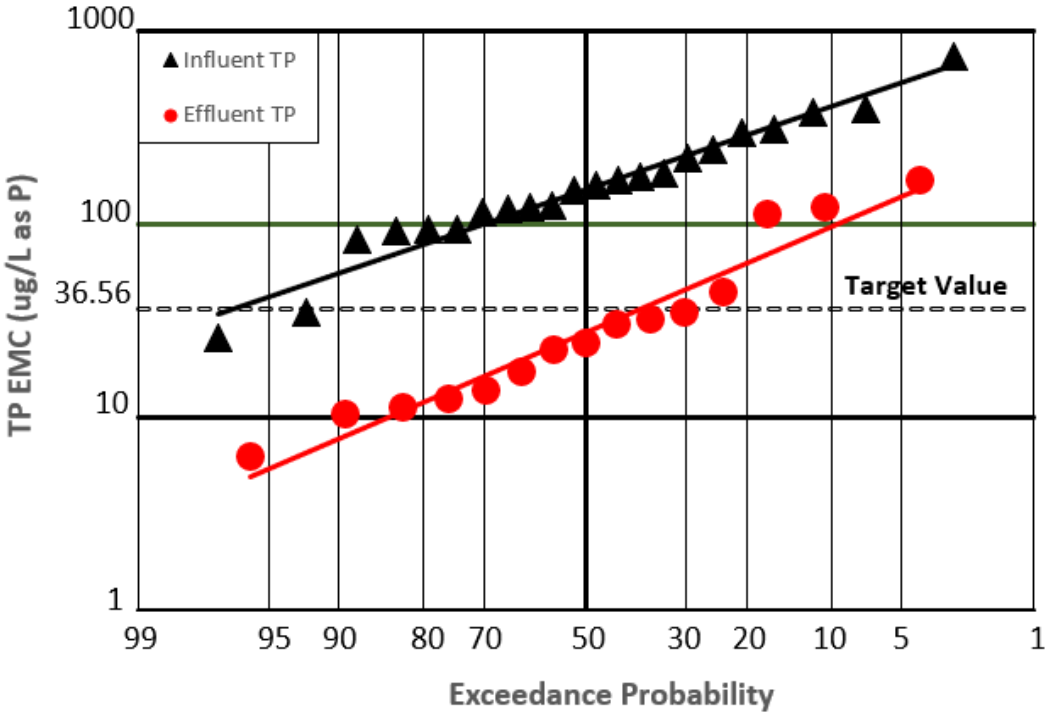

Figure 15. Exceedance probability plot of influent and effluent TP EMCs.

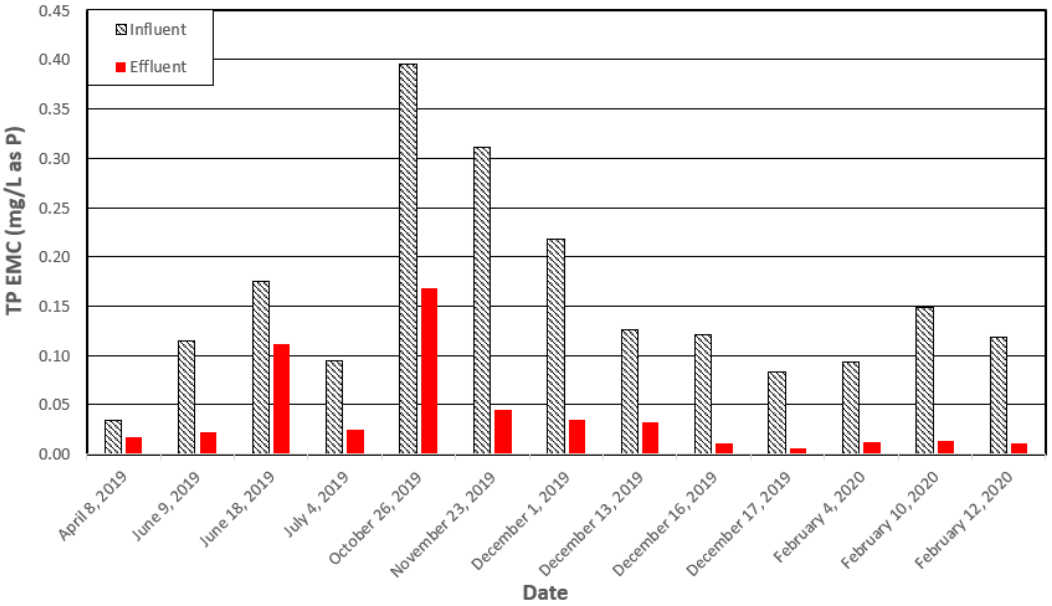

Figure 16. Influent and effluent TP EMCs for 13 paired-sample events.

In this study, the overall volume-weighted average influent TP EMC was calculated as 0.16 mg/L, which is lower than most of the EMCs found by other field studies (Urbonas 1999; Davis 2007; Hunt et al. 2008; Li and Davis 2009; Passeport et al. 2009; Barrett 2010; Liu and Davis 2013; Natarajan and Davis 2016; Doan and Davis 2017; Erickson et al. 2017). The Water Environment Federation and ASCE (WEF/ASCE 1998) reported that the EMC for total phosphorus in urban runoff is 0.33 mg/L. Brown et al. (2003) stated that a total phosphorus concentration of 0.3 mg/L is adequate to describe both new and old urban development. Some field studies found much higher overall volume-weighted average influent TP EMCs ranging from 0.5 to 0.8 mg/L (Davis et al. 2006; Brown et al. 2013). Stormwater runoff concentrations might be variable at different watersheds or under different rainfall characteristics. Some factors might affect the input TP: 1). land cover/land use since phosphorus sources varied from site to site; 2). rainfall depth, duration, intensity and antecedent dry days; 3). project duration because phosphorus inputs are affected by seasonality (Landsman and Davis 2018). In this project, more than half of the paired data are collected in winter (December to February), when the phosphorus sources were relatively limited. This may be the main reason why the input TP in this study is lower than other filed studies. However, the overall volume-weighted average TP EMC calculated using all influent samples (paired sample + non-paired sample) which covers more events from other seasons is 0.31 mg/L, which agrees with results in other field studies, and also meets the concentration in urban runoff reported by WEF/ASCE (1998) and Brown et al. (2003). The overall volume-weighted average

effluent TP EMC in this study was 0.042 mg/L, which corresponds to an 73.6% removal, indicating TP reduction was successfully achieved.

Particulate Phosphorus

The plunge pool shows a good PP removal as other EMCs. The individual influent PP EMCs ranged from 0.011 to 0.24 mg/L (median = 0.072 mg/L; 22 events), whereas the effluent ranged from <0.002 to 0.10 mg/L (median = 0.007 mg/L; 15 events). Figure 17 shows the exceedance probability plot for the influent and effluent PP EMCs. The plot illustrates about 82% effluent PP EMCs are less than 0.03656 mg/L, compared to only about 24% for the influent, which agrees with the common knowledge that traditional SCMs like biorientation and sand filters are highly effective at removing PP, relying on physical removal mechanisms such as sedimentation and filtration (Davis et al. 2006; Hsieh and Davis 2005; Davis 2007; Liu and Davis 2014; Landsman and Davis 2018).

Figure 18 shows the influent and effluent PP EMCs for 13 paired-sample events. All paired-sample events exhibited positive PP removal except the one collected on June 18, 2019. The EMC removal efficiencies ranged from 37.1% to 98.7% (median = 87.7%; 14 events) excluding the PP export event. The maximum influent PP EMC is 0.19 mg/L for the paired-sample events which found the same day as the maximum influent TP occurred. After passing through the plunge pool, the effluent PP EMC was reduced to 0.038 mg/L, corresponding to 80% removal. The Wilcoxon Signed-Rank Test also indicates that the effluent PP EMCs are significantly reduced compared with the influent (p-value = 0.00288). The overall

volume-weighted average influent PP EMC was 0.076 mg/L, compared to 0.014 mg/L for effluent after treatment, which means over 81.1% PP was removed by the plunge pool.

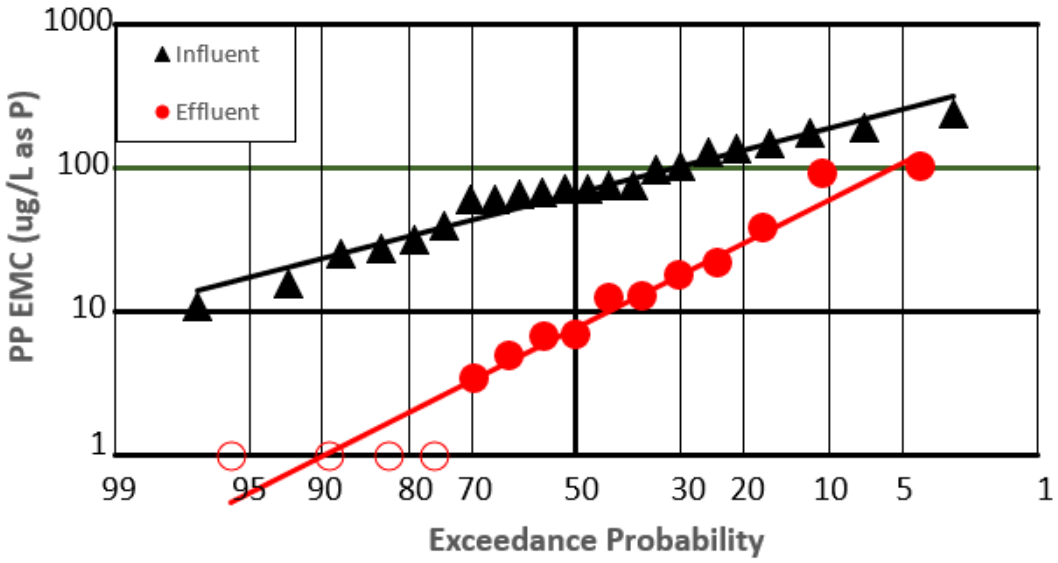

Figure 17. Exceedance probability plot of influent and effluent PP EMCs. Values below the detection limit are plotted as one half of the detection limit and are shown as open symbols.

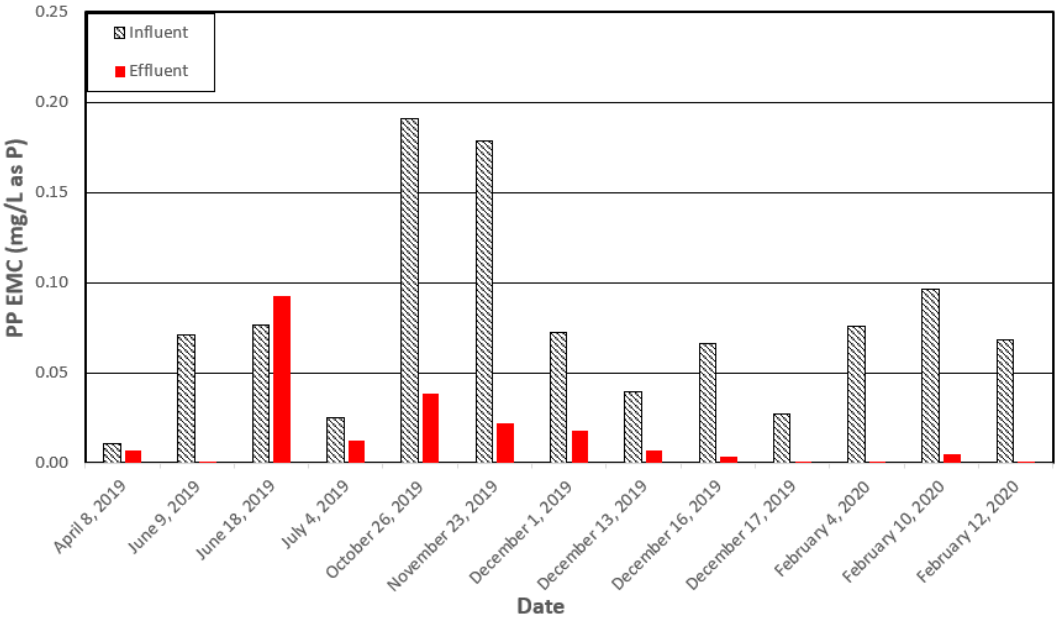

Figure 18. Influent and effluent PP EMCs for 13 paired-sample events.

Dissolved Phosphorus

The plunge pool shows satisfactory DP removal. The individual influent DP EMCs varied significantly, ranging from 0.01 to 0.49 mg/L (median = 0.062 mg/L; 22 events). After the runoff passed through the HFM, effluent DP EMCs decreased significantly; individual effluent DP EMCs lowered to 0.006 to 0.13 mg/L (median = 0.017 mg/L; 15 events). Figure 19 shows the exceedance probability plot for influent and effluent DP EMCs. More than 90% of effluent DP EMCs are less than 0.03656 mg/L, compared to about 27% for the influent, which indicates an effective DP reduction was achieved in the plunge pool.

Figure 20 shows the DP EMCs for 13 paired-sample events. All paired-sample events exhibited positive TP removal. The EMC removal efficiencies ranged from 27.7 to 88.7% (median = 80.7%; 13 events). The Wilcoxon Signed-Rank Test shows the difference between influent and effluent DP EMCs are statistically significant (p-value = 0.00148). The overall volume-weighted average influent DP EMC was 0.084 mg/L, compared to 0.028 mg/L in the effluent, which indicates 66.8% DP was removed.

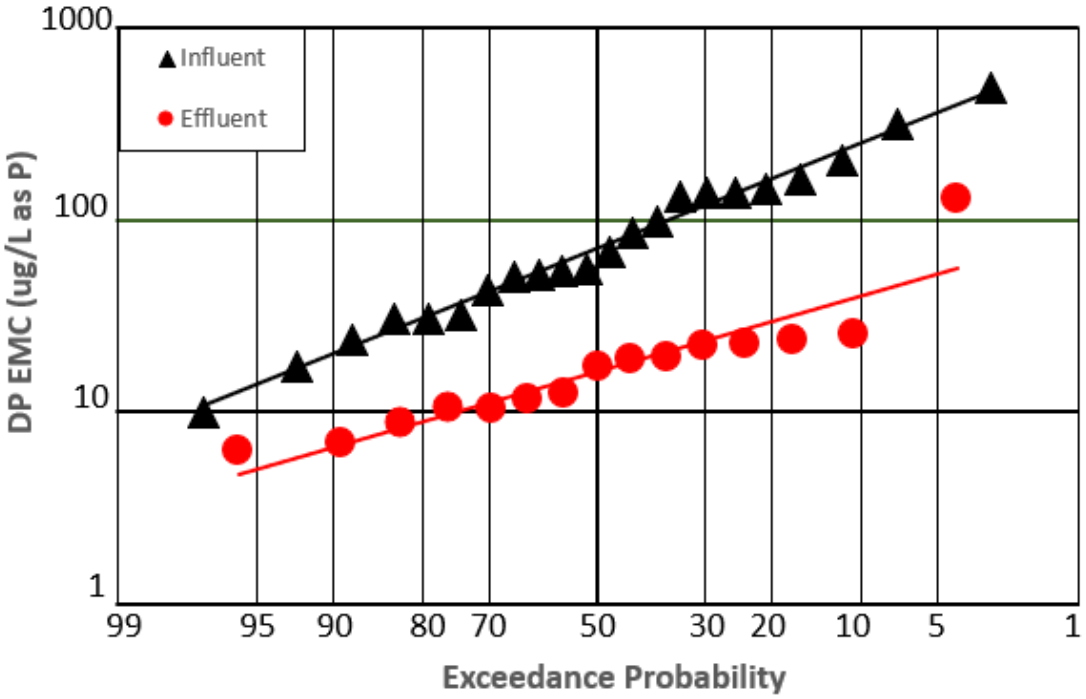

Figure 19. Exceedance probability plot of influent and effluent DP EMCs.

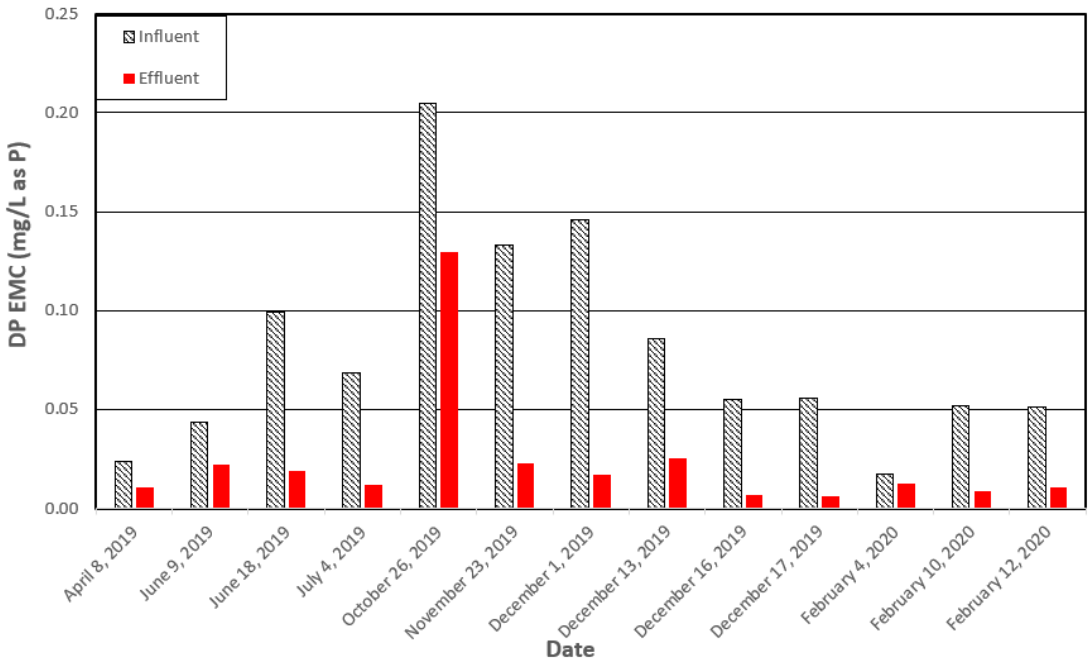

Figure 20. Influent and effluent DP EMCs for 13 paired-sample events.

The overall volume-weighted average dissolved fraction ($f_d = \frac{DP}{TP}$) was 0.53 in the influent, illustrating that phosphorus has almost equal fractions for DP and PP in the surface runoff, which is in accordance with results conducted in a residential area by Landsman and Davis (2018). However, the nationwide urban runoff program reports that the median EMC of TP and DP are 0.38 and 0.14 mg/L for residential land uses, respectively, indicating that a typical fraction of dissolved to total phosphorus can be expected to be approximately 37% (USEPA 1983). Other research (Pitt et al.2005; Berretta and Sansalone 2011; Liu and Davis 2013; Erickson et al. 2017) also found smaller DP fractions. It indicates that the DP fraction varies widely for different sites and storm events (Erickson et al. 2007). After passing through the plunge pool, the average DP fraction changed to 0.67 in the effluent.

SRP and DOP

The individual influent SRP EMCs varied from <0.002 to 0.16 mg/L (median = 0.038 mg/L; 22 events), and the effluent were from <0.002 to 0.05 mg/L (median = 0.01 mg/L; 15 events). Similar performance was noted for DOP, with an influent EMCs ranging from <0.002 to 0.33 mg/L (median = 0.025 mg/L; 22 events), and the effluent EMCs were consistently <0.002 to 0.08 mg/L (median = 0.005 mg/L; 15 events). Figure 21 and 22 show the exceedance probability plot for influent and effluent SRP and DOP EMCs. The plots show nearby constant outputs of SRP and DOP, which indicates adsorption is the main removal mechanism contributing to equilibrium concentration discharged from the plunge pool (Liu and Davis 2013).

The Wilcoxon Signed-Rank Test shows both the SRP (p-value = 0.00222) and DOP (p-value = 0.00438) EMCs reductions are statistically significant.

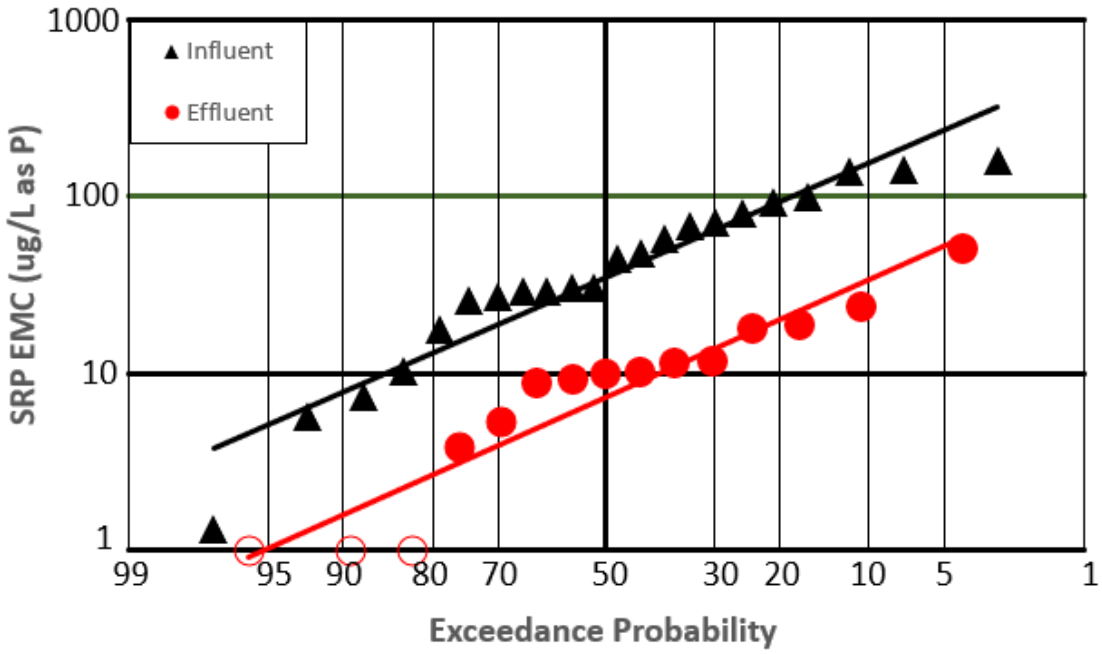

Figure 21. Exceedance probability plot of influent and effluent SRP EMCs. Values below the detection limit are plotted as one half of the detection limit and are shown as open symbols.

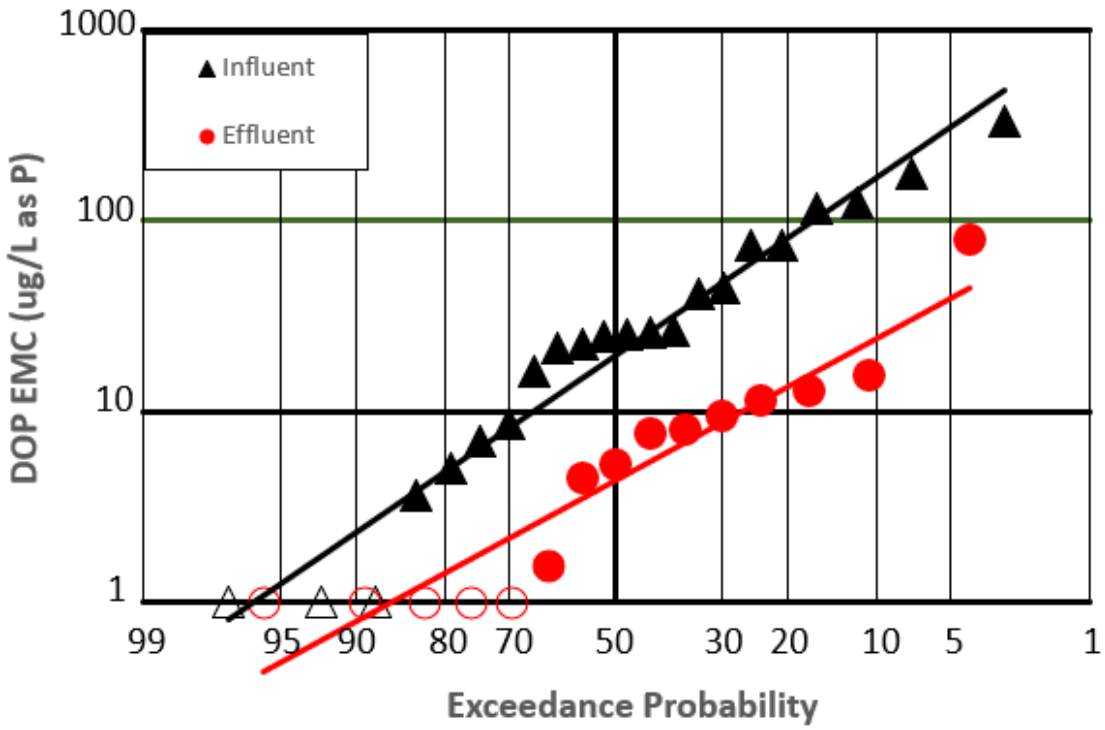

Figure 22. Exceedance probability plot of influent and effluent DOP EMCs. Values below the detection limit are plotted as one half of the detection limit and are shown as open symbols.

The nearly consistent low effluent DP EMCs indicates adsorption is the primary removal mechanism for DP. Given adequate time, P can find reactive sites in micropores of WTR, becoming more strongly adsorbed at individual surface sites (Ippolito et al. 2003). Some laboratory studies also found the similar steady state dissolved DP concentrations, which can be explained by the adsorption equilibrium mechanisms as well. For example, Erickson et al. (2012) found the influent DP EMCs varied from approximately 0.026-0.14 mg $PO_4^{3-} - P/L$ and the effluent EMC was consistently between a non-detect level (<0.01 mg $PO_4^{3-} - P/L$) and 0.023 mg $PO_4^{3-} - P/L$ using an iron enhanced sand filtration. O'Neill and Davis (2012) found the effluent DP EMC was always < 0.001 mg $PO_4^{3-} - P/L$ from input concentration

equal to 0.12 mg $PO_4^{3-} - P/L$ in a WTR bioretention amendment long-term column study.

Liu and Davis (2013) found constant outputs of SRP and DOP in the investigation of phosphorus removal by WTR retrofitted bioretention. Erickson et al. (2012) found a steady state dissolved DOP and SRP concentrations in the investigation of phosphate removal from synthetic stormwater by a sand filter amended with iron filings. Yan et al. (2016) also found the alum-modified WTR-BSM exhibits extremely high DOP and SRP sorption capacity based on the batch-scale experiments. The fractions of SRP and DOP are identical in the effluent, which suggests that same removal mechanisms are applied for SRP and DOP.

It was expected that the impact of baseflow could be eliminated using mass balance method. However, the iron particles in the baseflow had inevitable interferences to this project. Some complex chemical and physical reactions are likely between the iron particles and other materials when the two flows mixed. In fact, iron/iron oxide can reduce phosphorus concentration with similar mechanisms as WTR (aluminum and aluminum oxide). For example, phosphorus can be precipitated by iron and surface adsorbed to iron oxide (Erickson et al. 2007). In addition, iron-based materials have been shown to capture other pollutants including As, Cd, Cr, Cu, Ni, Pb, and Zn (Namasivayam and Ranganathan 1995; Genc-Fuhrman et al. 2008; Wu and Zhou 2009).

Therefore, the baseflow interference to phosphorus species (DP, PP, SRP, DOP) cannot be eliminated using the mass balance method. pH of the stormwater ranged from 6.34-7.98 in this study, and in this range the primary capture mechanism

for phosphates with iron is adsorption (Stumm and Morgan 1981). Phosphates bind to iron oxides by surface adsorption (Erickson et al. 2012). Reddy and D'Angelo (1994) also summarized: in mineral soils dominated by iron oxides, phosphate can be readily immobilized through sorption and precipitation by ferric oxyhydroxide, and formation of ferric phosphate can occur in the oxidized zones at the soil-water interface.

As shown in Figure 23, in the HFM, PP can be retained by sand particles, mostly via physical mechanisms like sedimentation and filtration; DP can be attached on the WTR surface and removed by adsorption mechanism. After passing through the HFM, the runoff flows into the outflow pipe and meets with the baseflow. The remaining DP from the treated runoff is adsorbed by iron/iron oxide particles and converted to PP. The baseflow works as a "second" treatment system by the iron/iron oxide, providing additional removal for DP. However, DP or PP cannot be retained in the outflow pipe, which means it is more like a conversion process (DP → PP) instead of a treatment/removal process. It decreases the DP fraction and increases the PP fraction (but TP remains constant). Furthermore, it is inconclusive which parts of DP were adsorbed, thus the baseflow impact on SRP and DOP speciation could not be eliminated by the mass balance method. All in all, the results of DP, PP, SRP, and DOP are inconclusive.

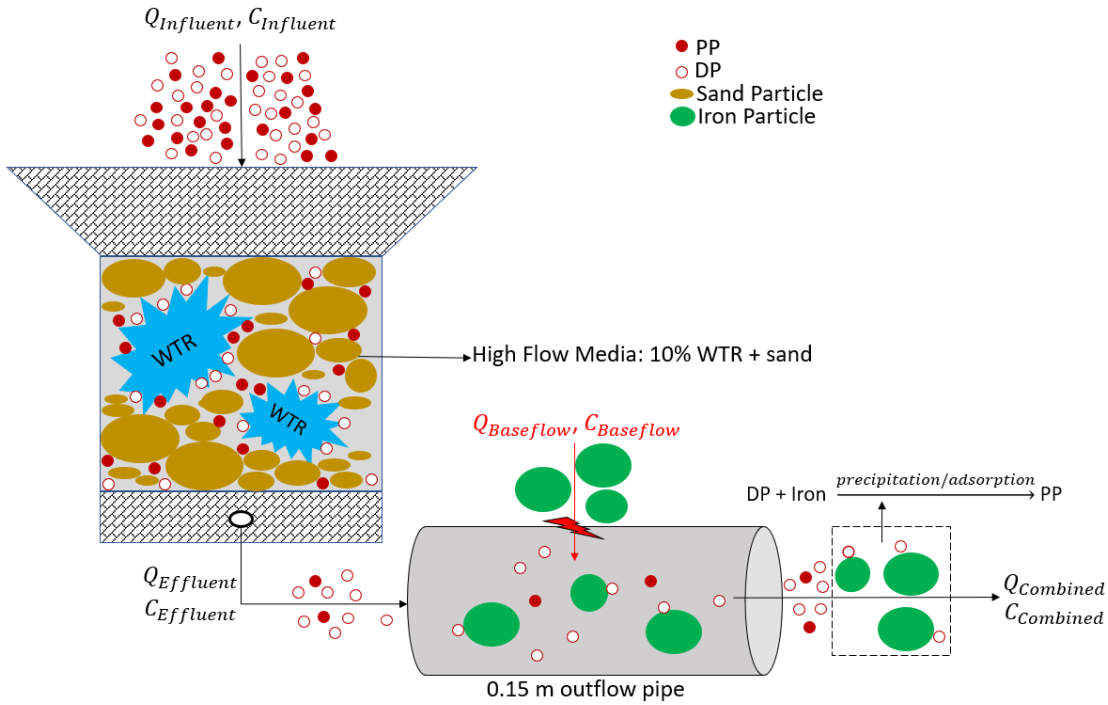

Figure 23. Stormwater runoff phosphorus behavior and fate in the WTR-incorporated HFM plunge pool system.

Literature Comparison

Field studies of phosphorus removal using WTR-related SCMs are sparse. The results are compared with the study of WTR retrofitted bioretention for phosphorus speciation and treatment conducted by Liu and Davis (2014), and the study of an iron enhanced sand filter to treat rainfall-induced agricultural tile drainage events conducted by Erickson et al. (2017). Also, comparisons are made with some traditional SCMs without WTR applied like bioretention and sand filters, to illustrate the significance of using WTR for phosphorus removal. There were also some pilot and laboratory studies that have learned that WTR incorporation increased phosphorus removal in SCMs.

One of the most comparable studies is the enhanced phosphorus removal bioretention retrofitted with 5% (by mass) WTR on the campus of the University of Maryland, conducted by Liu and Davis (2014). The overall volume-weighted average TP EMC was reduced from 0.3 to 0.11 mg/L (63% removal) by the WTR retrofitted bioretention, compared to 0.16 to 0.042 mg/L (73.8% removal) by the plunge pool. The influent TP in our study is about 50% less than Liu and Davis (2014), whereas the effluent TP is about 62% less. Since the effluent TP is much lower in our study (but the input is also lower), it suggests that the plunge pool has an excellent performance for TP management.

Another monitoring study measured the total phosphorus capture performance of an iron filings (6% by weight) enhanced sand filter installed to treat agricultural tile drainage (Erickson et al. 2017). The TP EMCs were reduced for all 20 collected events found in Erickson et al. (2017). The overall volume-weighted average influent TP EMC was 0.37 mg/L, which is 56.8% higher than we found. The higher TP EMC makes sense because the sand filter experimental site was designed to treat water from approximately 7.45 ha of farmland, which has more phosphorus input (fertilizer, herbicide) than the residential area in our project. The overall volume-weighted average effluent TP EMC was reduced to 0.125 mg/L after treatment, corresponding to a 66.2% reduction percentage, which shows satisfactory TP removal. Though the TP reduction percentage is higher in our study (73.8%), considering the higher input TP found by Erickson et al. (2017), the plunge pool might have a similar performance as the iron enhanced sand filter in TP removal.

Comparisons between the plunge pool and other traditional SCMs without WTR applied are conducted. The same bioretention experimental cell on the campus of the University of Maryland before WTR applied was studied by Li and Davis (2009). This study showed a less-effective performance for TP removal. TP leaching occurred from the media before the WTR incorporation (output > input), which might be attributed to specific media properties (Li and Davis 2009). As a common issue, TP export has been frequently found in traditional bioretention media. Hunt et al. (2006) observed that TP concentrations in the effluent of several bioretention facilities were higher than the influents and concluded that those bioretention media had high phosphorus contents, causing the TP export. Another large-scale WTR field test was conducted with bioretention soil mixes to evaluate phosphorous retention in Oregon by Poor et al. (2019). This study found that TP leaching from the traditional bioretention soil is a big issue, where the effluent TP concentrations were 6 to 20 times higher than influent. Bratieres et al. (2008) found P was also exported if 10% (by volume) leaf-compost and mulch is blended into the soil. Additionally, Dietz and Clausen (2005) also noted TP export from bioretention media in instances where the input phosphorus was very low.

There are several mechanisms of phosphorus removal in bioretention: filtration, sedimentation, adsorption, plant uptake, and microbial utilization. Microbial and plant uptake account for only a small fraction of P retained (Lucas and Greenway 2008). Traditional SCMs as bioretention and sand filters have a significant effectiveness to remove PP, relying on physical removal mechanisms like

sedimentation and filtration; however, DP will pass through the filter without treatment (Landsman and Davis 2018).

WTR offers a much greater phosphorus adsorption capacity with large specific surface area and abundant porous structure, which means more adsorption sites available for phosphorus attachment. In addition, the oxide/hydroxide aluminum and iron compounds in WTR bind with various phosphorus species as strong ligands, which may have a maximum phosphorus adsorption capacity of 25,000 mg-P/kg (Kim et al. 2002). Ligand exchange between the phosphate groups and the surface reactive hydroxyls of the adsorbents is the primary removal mechanism for both SRP and DOP (Parfitt et al. 1976; Shang et al. 1990, 1992). Improved SRP and DOP removal with alum addition can be attributed to the formation of high surface area aluminum hydroxide, which is an effective adsorbent for phosphorus (Anderson and Arlidge 1962; Hano et al. 1997) From a chemistry perspective, both Al and Fe are known as good Lewis acids and phosphate is a strong ligand/ Lewis base. As Lewis acides, Al and Fe cations have vacant orbitals which are able to accept electrons donated by phosphate; as such, phosphate can be taken up by WTR with high selectivity due to metal–ligand complexation (Qiu et al. 2019). That is why WTR incorporated SCMs can enhance phosphorus removal.

Some pilot and laboratory studies also have demonstrated that WTR incorporation can significantly increase phosphorus removal in bioretention. Recent laboratory work, using 15% WTR (by mass) employed as an amendment in a bioretention column, concluded that the TP was effectively removed from 4.0 to 7.0 mg/L in the influent to only 0.08 mg/L maximum in the effluent (Qiu et al. 2019),

which reached to over 98% removal efficiency. The value of 7.0 mg/L was an extremely high influent TP concentration, which is almost 15 times greater than the average TP EMC in urban areas. Under this extreme condition, the maximum TP concentration was only 0.08 mg/L in the effluent, which shows the significant ability of WTR for TP removal. Another long-term column study conducted by O'Neill and Davis (2012), showed that WTR-amended media far outperformed the non-WTR-amended control media for phosphorus management, in which the non-WTR-amended control column effluent TP EMCs were 7 to 30 times greater than the WTR-amended media TP EMCs under same conditions. The WTR-amended column showed consistent removal of P from synthetic stormwater, with TP EMCs ranging from < 0.01 to 0.025 mg/L, compared to 0.12 mg/L influent TP EMC (O'Neill and Davis 2012). These laboratory studies indicate that the WTR significantly enhances TP removal capacity for bioretention systems under either low or high input TP conditions. Though laboratory studies were conducted under controlled conditions, the results are valuable references to the EMCs designs.

Nitrogen

Total Nitrogen

The plunge pool did not show an effective TN removal. Figure 24 shows the exceedance probability plot of influent and effluent TN EMCs. Variation among TN was noted, most likely due to seasonal variation of fertilizer application and leaf decay, among other factors (Landsman and Davis 2018); the individual influent TN

EMCs varied from 0.53 to 3.6 mg/L (median = 1.6 mg/L; 14 events), whereas the effluent varied from 0.26 to 4.0 mg/L (median = 0.95 mg/L; 12 events). About 30% of the effluent EMCs are less than the EPA water quality criterion of 0.69 mg/L (USEPA 2000), compared with 10% in the influent, which is not a big improvement.

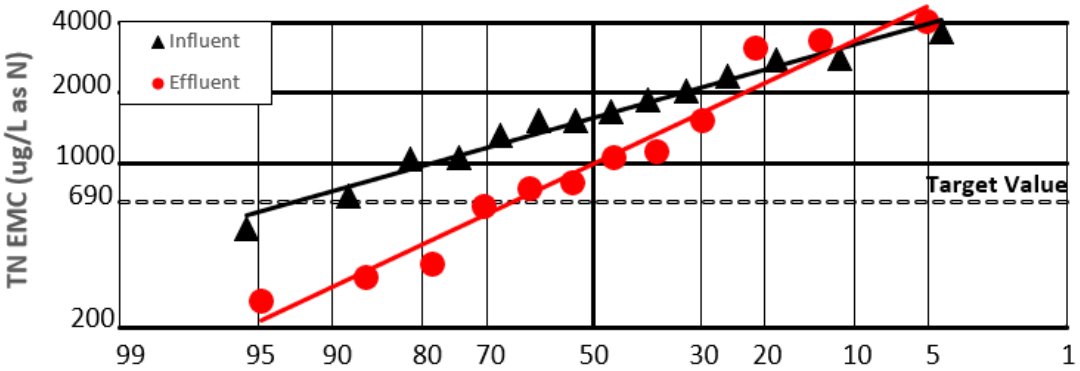

Figure 24. Exceedance probability plot of influent and effluent TN EMCs.

The overall volume-weighted average influent TN EMC is 1.41 mg/L, which is within the range reported by Collins et al. (2010) that average TN EMCs in stormwater for urban land uses are between 1.3 and 3.2 mg/L as N. The overall volume-weighted average effluent TN EMC is 1.35 mg/L, corresponding to only 4.3% removal. Nitrogen fate in the plunge pool is complex and difficult to treat because varies nitrogen forms including $NO_3^- - N$, $NO_2^- - N$ and $NH_4^+ - N$ exist and several treatment mechanisms like sedimentation, filtration, adsorption and mineralization are operative in the system (Davis et al. 2006; Hatt et al. 2007; Cho et al. 2009; Brown et al. 2013). The nitrification process $NH_4^+ \rightarrow NO_2^- \rightarrow NO_3^-$ leads to nitrate export, which might be the main cause of the poor performance.

Nitrogen has not been the focus in the WTR retrofitted studies (Lucas and Greenway 2011; Liu and Davis 2014; Erickson et al. 2017), but typically nitrogen export was ascribed to other N-containing sources. However, WTR might be a significant nitrogen source; other studies have reported that WTR contains up to 500 mg-N/kg (Dayton and Basta 2001; Lei and Davis 2019). TN removal efficiency is highly varied with SCM studies. Urbonas (1999) found the overall volume-weighted effluent TN EMC was reduced from 8.0 to 3.8 mg/L in a sand filter study. Barrett (2010) found similar results as our study in the evaluation of sand filter performance in Texas, with overall volume-weighted average influent and effluent TN EMCs as 1.5 and 1.1 mg/L as N. Li and Davis (2008) reported the overall volume-weighted average influent and effluent TN EMCs are 3.1 and 2.4 mg/L in a traditional bioretention in University of Maryland. Li and Davis (2014) reported minimal capability of decreasing TN concentrations in stormwater runoff using traditional bioretention, with the overall volume-weighted average influent and effluent TN EMCs equaling to 1.62 and 1.55 mg/L. This variability of TN removal in different studies is due to the complexity of nitrogen behavior in bioretention and sand filtration systems, because nitrogen has a diverse speciation in runoff and its speciation and concentration varies with site and season (Taylor et al. 2005).

Nitrate and Nitrite

Figure 25 shows the exceedance probability plot of influent and effluent $NO_3^- - N$ EMCs. The range of $NO_3^- - N$ EMCs varied greatly, with the influent varying from <0.002 to 1.6 mg/L (median = 0.095 mg/L; 15 events) and the effluent

from <0.002 to 2.3 mg/L (median = 0.146 mg/L; 12 events). As the probability plot shows, the effluent trend line is above the influent, which illustrates $NO_3^- - N$ export. Poor $NO_3^- - N$ removal was attributed to internal assimilation/release processes and possibly from direct transformation of runoff nitrogen, specifically, to the conversion of captured $NH_4^+ - N$ and $NO_2^- - N$ into $NO_3^- - N$ between storm events (Landsman and Davis 2018). Similar results were found in other bioretention studies (Kim et al. 2003; Hsieh et al. 2007; Li and Davis 2008; Zinger et al. 2013; Li and Davis 2014; Landsman and Davis 2018), which conclude that $NO_3^- - N$ is highly mobile and will generally wash straight through an aerobic sand filter and/or bioretention cell. Nitrogen removal varies among the systems, but in general, mineralization and nitrification of accumulated nitrogen species in the SCMs leads to nitrate export (Landsman and Davis 2018). $NO_2^- - N$ was rarely detected in the plunge pool. Hunt et al. (2008) reported for SCM systems which did not employ a designed saturated zone, or internal water storage (IWS) zone, the lack of $NO_3^- - N$, $NO_2^- - N$ reduction is expected. Some SCM studies (Hunt et al. 2006; Hsieh and Davis 2005; Dietz and Clausen 2006) found that the removal of $NO_3^- - N$, $NO_2^- - N$ increased with the presence of an internal water storage layer or "designed" saturation zone.

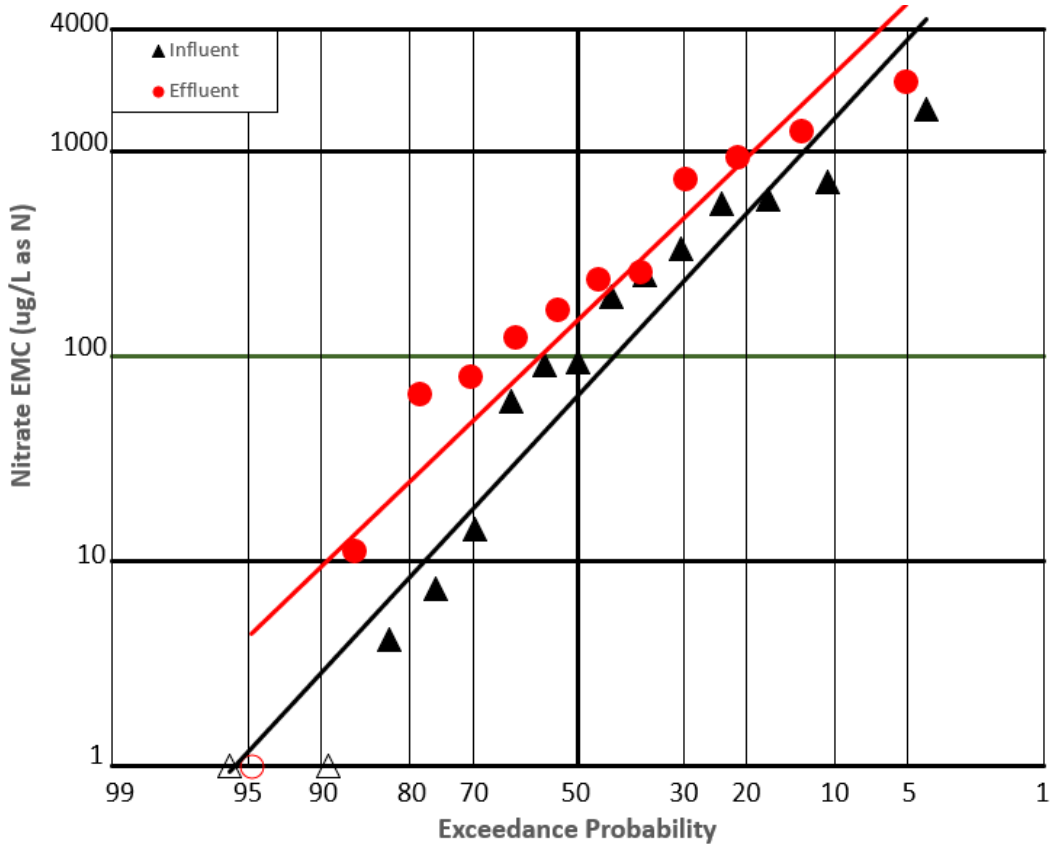

Figure 25. Exceedance probability plot of influent and effluent $NO_3^- - N$ EMCs. Values below the detection limit are plotted as one half of the detection limit and are shown as open symbols.

Ammonium

$NH_4^+ - N$ removal was detected in the plunge pool. Figure 26 shows the exceedance probability plot of influent and effluent $NH_4^+ - N$ EMCs. The influent $NH_4^+ - N$ EMCs ranged from <0.003 to 0.52 mg/L (median = 0.091 mg/L; 15 events), whereas the effluent varied from <0.003 to 0.174 mg/L (median = 0.015 mg/L; 12 events). The relatively low $NH_4^+ - N$ EMCs and high $NO_3^- - N$ in the effluent indicates nitrification might be the major removal mechanism for $NH_4^+ - N$ removal in the system, $NH_4^+ - N$ is nitrified to $O_3^- - N$ under aerobic conditions

during drying between storm events (Chen et al. 2006; Hatt et al. 2007; Cho et al. 2009). Moreover, NH_4^+ fixation and ion exchange might happen by the aluminum hydroxide in the WTR or hydrated oxides of iron in the baseflow (Dipankar and Asit 1981; Uttam and Katsuhiro 1997).

$NH_4^+ - N$ removal in stormwater runoff has been reported in some other SCM studies. Hunt et al. (2008) found that the mean concentration of $NH_4^+$was reduced from 0.34 mg/L to 0.1 mg/L as N (below the reporting limit) by a bioretention cell in urban Charlotte, NC, attributing removal to combined sorption-nitrification processes. Li and Davis (2014) found the volume-weighted average $NH_4^+ - N$ EMC was significantly reduced from 0.15 to <0.05 mg/L (below detection limit) at the University of Maryland.

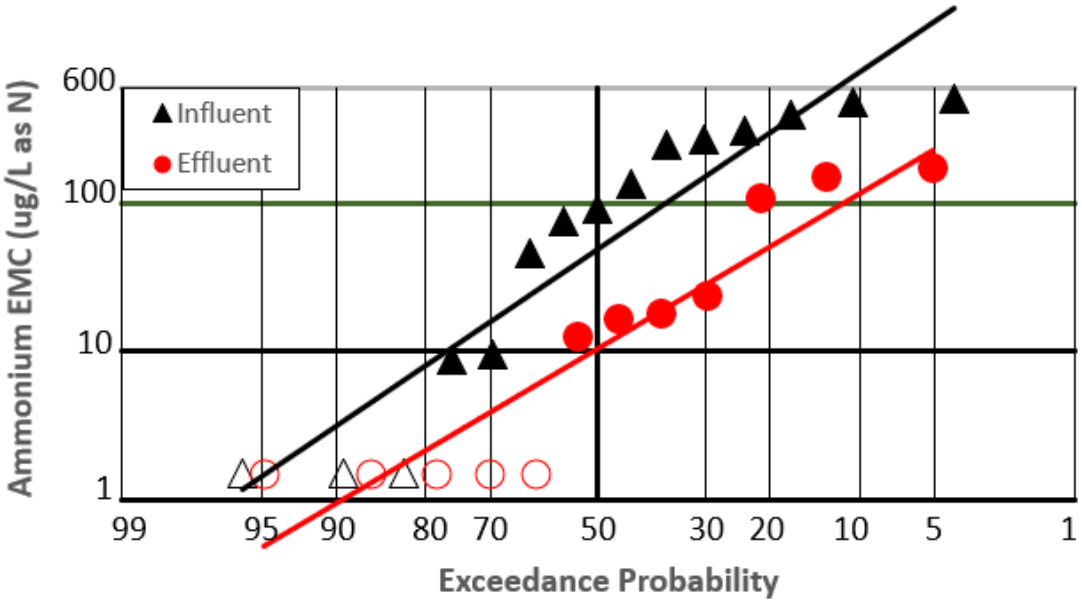

Figure 26. Exceedance probability plot of influent and effluent $NH_4^+ - N$ EMCs. Values below the detection limit are plotted as one half of the detection limit and are shown as open symbols.

Metals

A metal of significant concern for leaching from the plunge pool is aluminum, because the media was created using aluminum-based WTR. Another study using Al WTR (Ostrom and Davis, 2019) found aluminum concentration increased from influent to effluent in earlier storm events, which might have been caused by initial washout of fines containing powdered WTR as the media was newly established.

In this study, the total aluminum EMC ranged from 0.052 to 1.31 mg/L (median = 0.434 mg/L) for the influent, whereas it was 0.001 to 0.33 mg/L (median = 0.046 mg/L) for the effluent (Table1). As Figure 27 shows, all effluent EMCs are less than the influent except the event on November 18, 2019, which indicates that aluminum leaching is not a concern in this project. A relatively large rainfall (0.58 cm) with large amount of influent runoff (186 m^3) in that event might be the possible reason for the high aluminum concentration from the media. Almost all the influent (12 events) EMCs exceeded the EPA ambient water quality criterion for aluminum, 87 µg/L, for freshwater at pH between 6.5 and 9.0 (USEPA, 1988). After passing through the WTR media, ten of the effluent EMCs were below the EPA criterion and only three exceeded. The aluminum in the particulate phase has the same trend as total aluminum. Only one of the paired events shows that the concentration increased from the influent to effluent.

Table 5. Metal data of 13 monitored stormwater events at the WTR-incorporated HFM plunge pool experimental site.

		Influent EMC (mg/L)		Effluent EMC (mg/L)	
Metal	N (Number of Events)	Range	Median	Range	Median
Total Aluminum	13	0.052-1.31	0.434	0.025-0.33	0.046
Total Iron	13	0.064-17.4	0.546	0.025-59.1	7.41
Total Zinc	13	0.025-0.062	0.044	0.025-0.032	0.025
Total Copper	13	0.005-0.013	0.009	0.005-0.026	0.007

For the aluminum in the dissolved phase, most of the EMCs (9 for influent; 12 for effluent) were below the 25 µg/L detection limit; only one effluent sample was found above 25 µg/L. The results agree with aluminum solubility calculations, which is about 9 µg/L ($10^{-6.5}$ M total Al) at pH 6 and 8 (Stumm and Morgan 1996; Ippolito et al. 2011). It can be concluded that aluminum leaching is not an issue in this project.

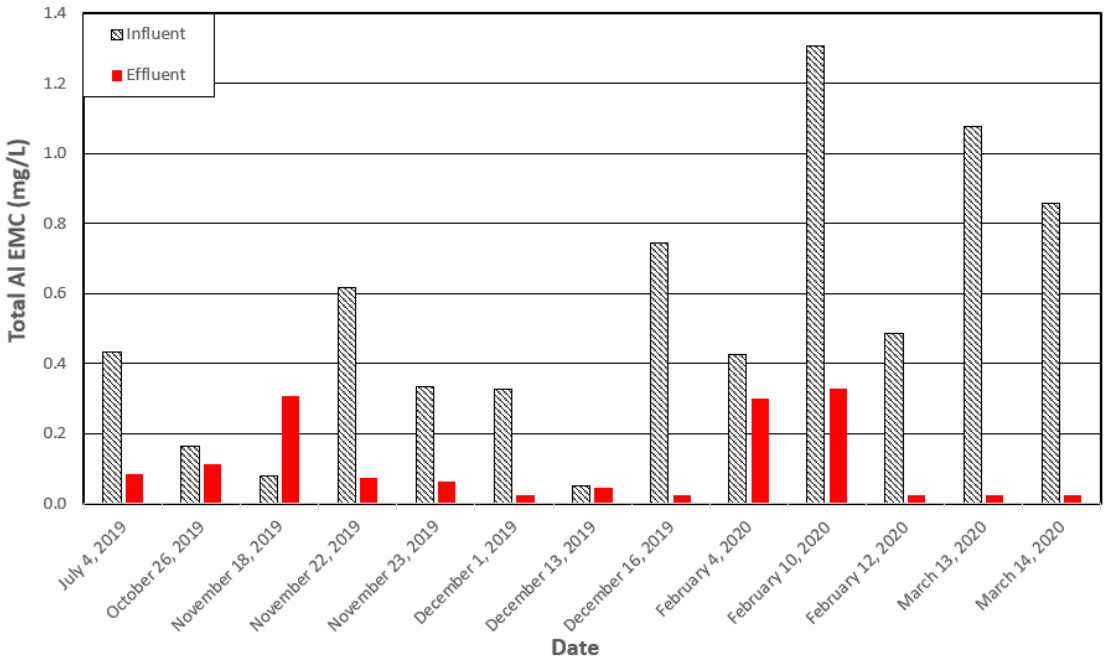

Figure 27. Influent and effluent total aluminum EMCs for 13 paired-sample events. Data below the detection limit are plotted at the detection limit of 25 µg/L.

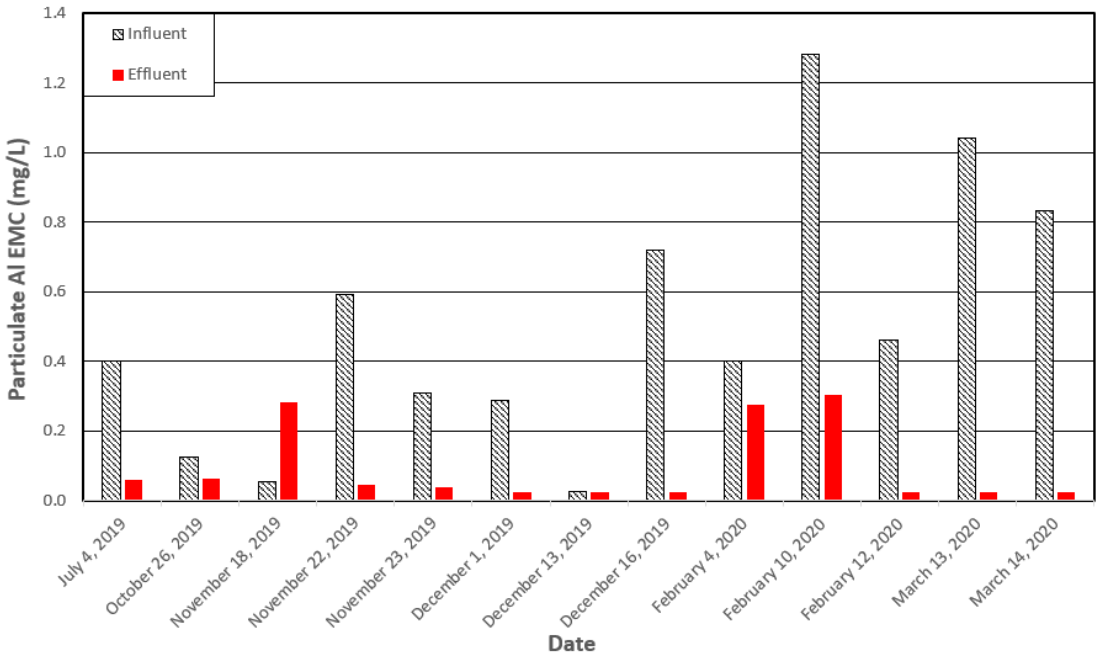

Figure 28. Influent and effluent particulate aluminum EMCs for 13 paired-sample events. Data below the detection limit are plotted at the detection limit of 25 µg/L.

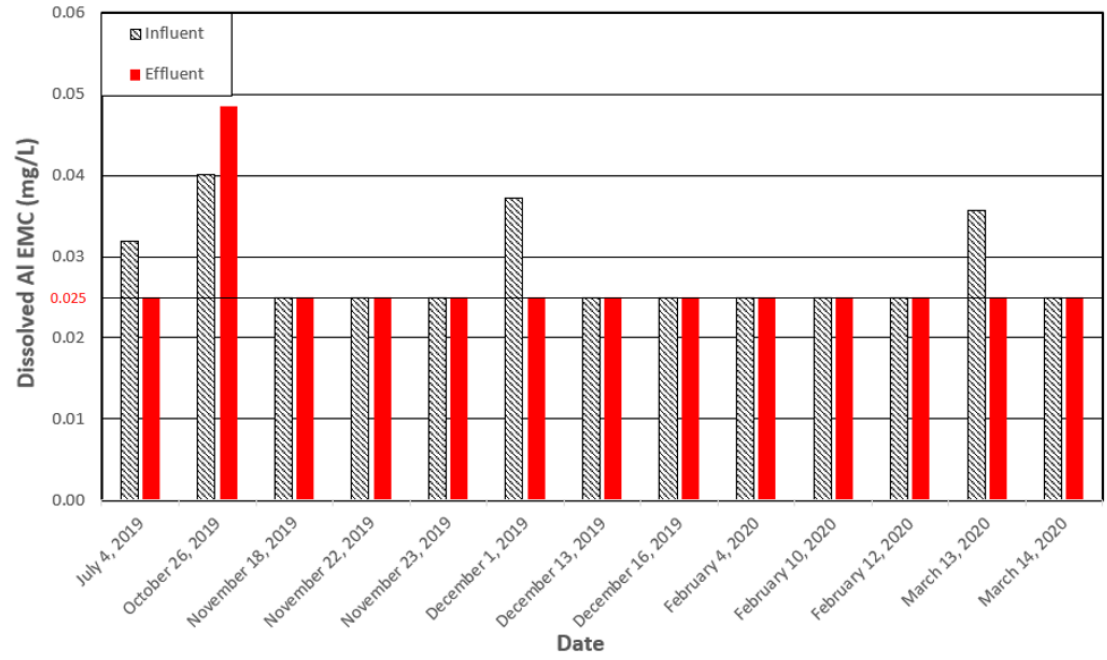

Figure 29. Influent and effluent dissolved aluminum EMCs for 13 paired-sample events. Data below the detection limit are plotted at the detection limit of 25 µg/L.

Figure 30 shows that the influent iron concentrations are relatively low, most of them are lower than the EPA ambient water quality criterion for Fe at 1000 µg/L

(USEPA, 1986). The effluent iron concentrations were expected to be lower than the influent since no leaching was found from the media based on the aluminum data. However, the effluent data were affected because of the extremely high iron concentrations from the baseflow. Two events show very high effluent iron concentrations (54.5 mg/L and 59.1 mg/L). The main reason for variation is the rainfall/effluent characters. Relatively small rainfall leads to small effluent volumes, which means the difference between the effluent volume and baseflow volume is small. The volume difference was used as a denominator in the mass balance calculations, and the small denominator led to a high result, which caused some bias. Most of the total iron EMCs (9 events) exceeded the EPA criterion for the effluent. Most of the iron EMCs (9 for influent; 8 for effluent) in the dissolved phase are below the 25 µg/L detection limit. But iron export was detected for both total iron and dissolved iron. The high iron concentrations in the effluent were caused by improper function of the facility. This site will require extra work to remove the baseflow iron and prevent further contamination.

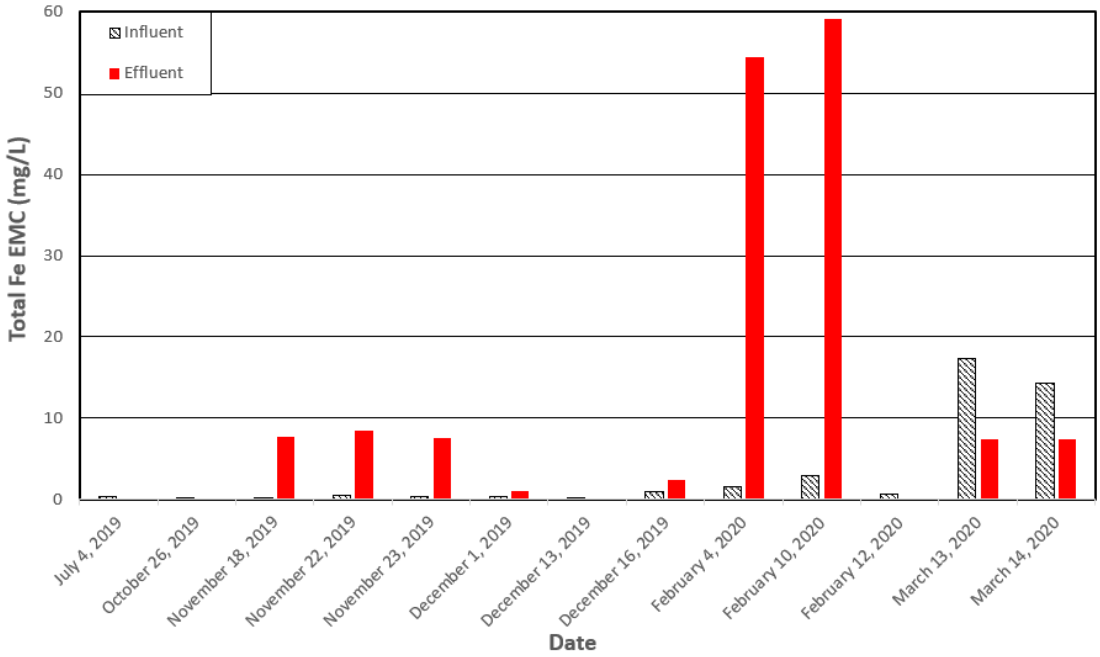

Figure 30. Influent and effluent total iron EMCs for 13 paired-sample events. Data below the detection limit are plotted at the detection limit of 25 µg/L.

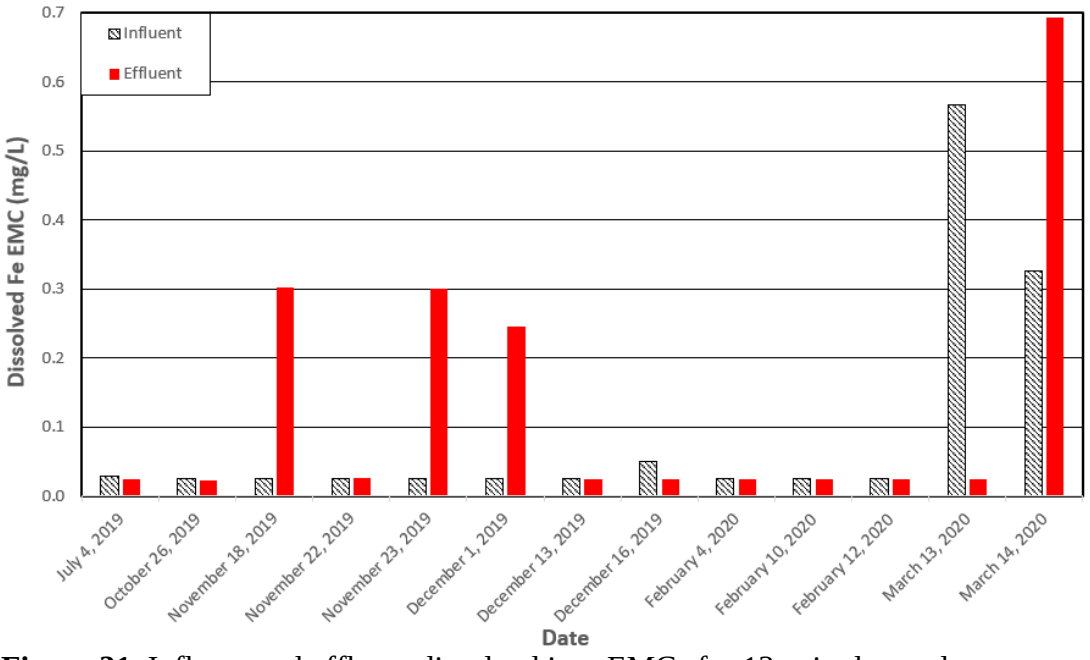

Figure 31. Influent and effluent dissolved iron EMCs for 13 paired-sample events. Data below the detection limit are plotted at the detection limit of 25 µg/L.

Figure 32 shows an effective and consistent zinc removal by the plunge pool system. The total zinc EMCs in the effluent are less than the influent for all 13 events. Even with very low influent total zinc concentrations, the WTR still shows excellent ability for zinc removal. All the influent concentrations are below the 133 µg/L EPA criterion for acute toxicity to the freshwater aquatic life (USEPA, 1996). After passing through the WTR media, almost all (12 events) effluent total zinc concentrations are lowered to less than the 25 µg/L detection limit, which indicates very good performance. The removal of zinc can be attributed to the complexation with aluminum oxides in the WTR (Castaldi et al., 2015).

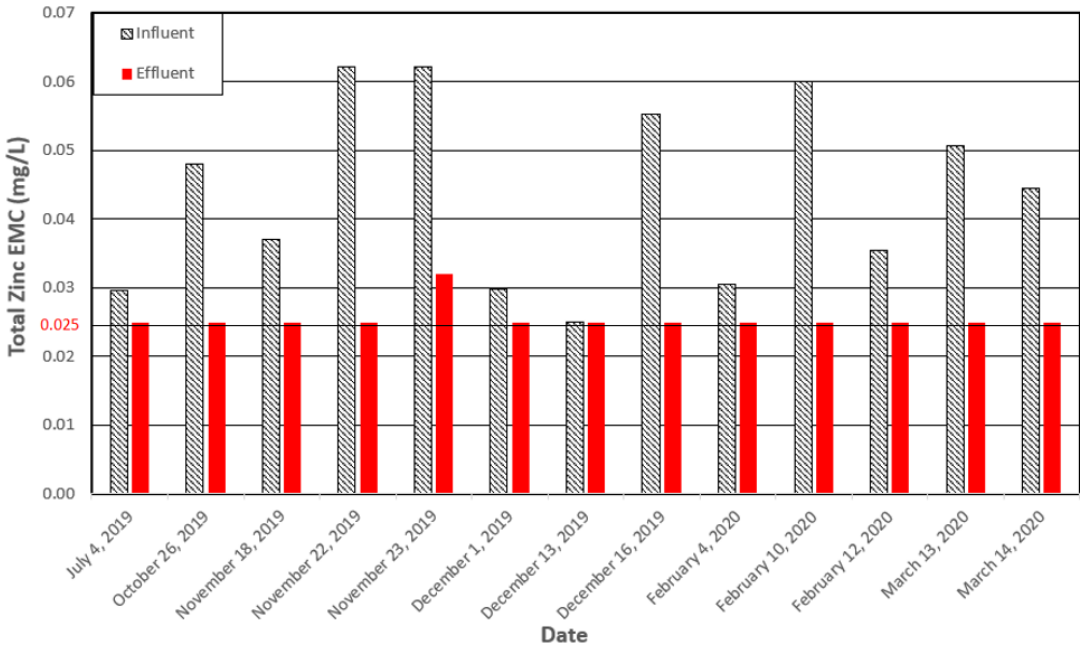

Figure 32. Influent and effluent total zinc EMCs for 13 paired-sample events. Data below the detection limit are plotted at the detection limit of 25 µg/L.

The concentrations of copper are low for both influent and effluent. The total copper EMC ranged from <0.01 to 0.013 mg/L (median = 0.009 mg/L) for the influent, whereas it was <0.01 to 0.021 mg/L (median = 0.007 mg/L) for the effluent (Table 5). Six events had copper removal from influent to effluent, and the effluent EMCs are below the 13 µg/L EPA criterion for acute toxicity to freshwater aquatic life. However, six events showed copper export and four of had effluent EMCs in excess of the toxicity criterion.

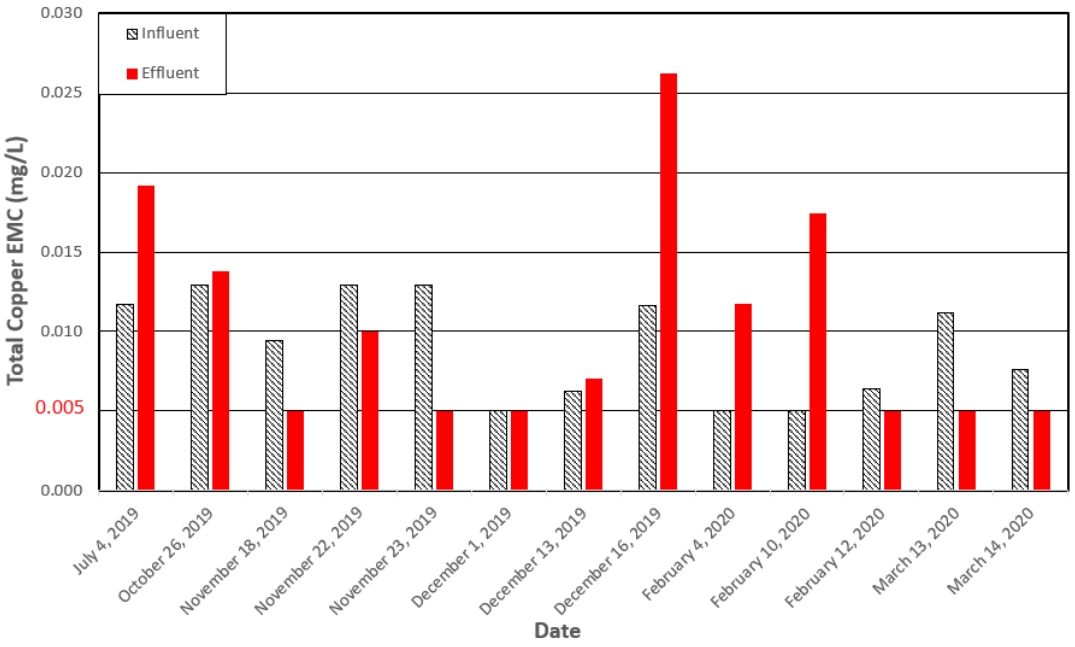

Figure 33. Influent and effluent total copper EMCs for 13 paired-sample events. Data below the detection limit are plotted at half the detection limit of 10 µg/L.

Different factors in a water body can affect metals toxicity, for example, pH, hardness, alkalinity, and organic matter concentrations (Ostrom and Davis, 2019). It can be concluded that aluminum leaching is not a concern in this project under conditions typical of stormwater runoff. The high iron concentrations in the effluent are attributed to the failure of the effluent pipe system and the baseflow. The WTR

media can remove zinc effectively, leading to effluent concentrations that meet EPA water quality standards. The WTR media had a decent performance of copper removal. The effluent EMCs are between 0.005 to 0.021 mg/L, and six events showed positive removal.

Pollutant Mass Load Reduction

Pollutant mass load reductions for stormwater passing through the plunge pool consists of two parts: 1). pollutant concentration reduction; 2). volume reduction. These reductions can be envisioned as follows: 1). when runoff flows into the plunge pool, treatment (precipitation and adsorption) takes place at the media surface (Li and Davis 2008) designated as system treatment, which is concentration reduction; 2). stormwater volume is reduced by percolation, storage, and/or evapotranspiration, which is volume reduction (Liu and Davis 2013).

The input and discharge annual pollutant mass loads per unit drainage area (L, in kg/ha/yr) were calculated to determine the overall treatment effectiveness of the plunge pool using Equation 15:

$$L = \frac{MP}{AD} \qquad Eq.15$$

where M is overall cumulative input/output pollutant mass (kg) measured during this study; P is the average annual precipitation [107 cm/year for the State of Maryland; Maryland Department of the Environment (MDE) 2011]; A is the effective drainage area (ha) [2.898 ha for the experimental site]; and D is the total precipitation depth (cm) measured during the entire monitoring duration. The annual pollutant mass

reduction entirely due to volume reduction, L_{V-red} was computed by Eq.16, as the cumulative sum of the product of measured effluent EMCs and runoff volume reductions (difference between influent and effluent volumes). If no discharge occurred, the entire mass reduction was attributed to volume reduction for that event.

$$L_{V-red} = \sum_{i=1}^{i=n} EMC_i * (V_{in(i)} * V_{out(i)}) \qquad Eq.16$$

The overall pollutant mass load reduction ratio, R_m, was calculated using Eq. 17:

$$R_m = \frac{L_{in} - L_{out}}{L_{in}} \qquad Eq.17$$

where L_{in} is the input pollutant load, and L_{out} is the output pollutant load. The mass volume reduction ratio, R_{m-V}, accounts for the fraction of L_{V-red} (volume) responsible for the total mass reduction, was calculated by:

$$R_{m-V} = \frac{L_{V-red}}{L_{in} - L_{out}} \qquad Eq.18$$

Table 6. Overall Volume-Weighted Average EMCs and Annual Pollutant Mass Loads at the WTR-Incorporated HFM Plunge Pool.

	Overall Volume-Weigthed Average EMC (mg/L)		Annual Mass Load ($kg/ha-yr$)			Percent Mass Reduction	
Pollutant	Influent	Effluent	L_{in}	L_{out}	L_{V-red}	R_m	R_{m-V}
TSS	50	18	114	8	44	93.2%	41.3%
TP	0.160	0.042	0.37	0.02	0.06	95.0%	18.0%
PP	0.076	0.014	0.18	0.01	0.03	96.4%	16.9%
DP	0.084	0.028	0.19	0.01	0.04	93.7%	19.4%
SRP	0.049	0.014	0.11	0.01	0.03	94.5%	24.7%
DOP	0.035	0.014	0.08	0.01	0.01	92.7%	12.8%
TN	1.41	1.35	5.05	0.66	2.67	86.9%	61.0%
$NO_3^- - N$	0.42	0.57	1.09	0.20	0.39	81.7%	44.0%
$NH_4^+ - N$	0.11	0.05	0.29	0.02	0.24	94.1%	86.9%

Note: Overall volume-weighted average EMCs were calculated by cumulative mass divided by the cumulative volume for all collected samples.

The overall influent and effluent volume-weighted average EMCs, annual pollutant mass loads and pollutant mass reduction ratios for all phosphorus species are summarized in Table 4. Both EMCs and mass loads were reduced for TSS and all P species. Moreover, percentage mass reductions are higher than the EMC percentage removals due to the attenuation of volume by the HFM. The volume reductions have a small contribution to phosphorus and phosphorus species mass reductions (less than 25%), but it contributes a lot for TSS mass reduction (41.3%) and nitrogen species mass reductions (over 40%). TSS mass was reduced from 114 to 7.8 kg/ha-yr, corresponding to 93.2% mass reduction. TP mass was reduced from 0.37 to 0.02 kg/ha-yr, corresponding to 95% mass reduction. In comparation, Liu and Davis (2014) found TP mass was reduced from 3.0 to 0.48 kg/ha-yr in the WTR retrofitted bioretention, corresponding to 84.0% mass reduction. Comparing the mass reduction ratios from these two studies, the plunge pool has a better performance for TP load reduction. However, the input TP load from Liu and Davis (2014) was much higher than ours, and it still achieved an 84% mass reduction, which means the WTR retrofitted bioretention is very effective for TP removal as well. Erickson et al. (2017) found the TP load was reduced by 66.3% from 1.27 kg to 0.43 kg in the iron filings enhanced sand filter, which shows satisfactory treatment as well.

Other traditional SCMs showed much lower mass reduction ratios or even mass exports. Hunt et al. (2006) found a substantial TP export from the bioretention systems in one of the field sites in North Carolina, which had 0.13 kg input mass and 0.44 kg output mass, corresponding to 240% increase. In addition, Dietz and Clausen (2005) noted TP mass export from bioretention media in instances where the input TP

was very low, which had 7.16 g TP input and 15.09 g TP output, corresponding to 110.6% increase. Li and Davis (2009) found input and output TP loads were 2.7 and 1.2 kg/ha-yr (55% reduction) in the same bioretention before WTR retrofit; Li and Davis (2009) reported input and output TP were 0.9 and 0.38 kg/ha-yr (58% reduction) in another traditional bioretention system. After application of WTR, the mass reduction increased significantly, which supported that WTR incorporation enhanced P sorption capacity of the media, resulting in a more effective TP treatment.

Other P species have excellent load reductions as well. PP, DP, SRP, DOP have over 90% mass reduction ratios. Similar fractions of DP and PP were found both in the input and output, which suggests the plunge pool can remove the dissolved and particulate phosphorus effectively. SRP (58.3%) has a little higher fraction than DOP (41.7%) in the influent, but the same fractions of DOP and SRP were found in the effluent, which suggests that they were removed by similar sorption mechanisms (Liu and Davis 2013).

TN mass was reduced from 5.05 to 0.66 kg/ha-yr, which achieves 86.9% mass reductions, mostly attributed to the volume reduction (61%). Volume reductions also contribute a lot to mass reductions for other N species. $NO_3^- - N$ had an 81.7% mass reduction, where 44% is from volume reduction; and $NH_4^+ - N$ had an 94.1% mass reduction, where 86.9% is from volume reduction.

Chapter 4: Conclusions

To minimize the pollutant loads entering water bodies from stormwater, a WTR-incorporated HFM plunge pool was installed as a SCM in a residential community in Maryland, USA. During the research period, 25 stormwater events were monitored. Water quality performance of the plunge pool was evaluated by analyzing the influent and effluent pollutants concentrations including TSS, phosphorus, nitrogen and metals. However, there was an effluent seepage caused a "baseflow" in the downstream pipe, which was a significant challenge in this project. The plunge pool had a satisfactory performance for TSS removal via sedimentation and filtration, which reduced the overall volume-weighted average EMC from 50 to 18 mg/L. Substantial mass load reduction (93.2% percentage reduction) was achieved in TSS, whereas 41.3% was attributed to volume reduction. TSS exports were exhibited in 3 storm events, which might be imputed to the iron particles from the baseflow. Excellent phosphorus removal was achieved as expected. All paired-sample events (13 events) exhibited positive TP removal, and TP EMCs were significantly reduced with the overall volume-weighted average EMC equaling 0.16 mg/L in the influent, compared to 0.042 mg/L in the effluent. 95% TP mass load was removed after the runoff passing through the plunge pool, with 82% attributed to the EMC reductions. The overall volume-weighted average influent PP and DP EMCs were 0.076 and 0.084 mg/L, comparing 0.014 and 0.028 mg/L in effluent after treatment. The iron/iron oxide from the seepage further converted DP to PP in the downstream pipe, which makes DP, PP, SRP and DOP results inconclusive.

TN removal was less effective in the plunge pool system, with overall volume-weighted average EMCs equaling 1.41 mg/L for the influent and 1.35 mg/L for the effluent, most likely due to $NO_3^- - N$ export from the system through mineralization and nitrification process (Landsman and Davis 2018). This result suggests that WTR does not have a significant effect on N concentration.

Dissolved aluminum leaching from the system was less than 0.05 mg/L. The high iron concentrations in the effluent are attributed to the failure of the effluent pipe system and the baseflow. The WTR media can remove zinc effectively, leading to effluent concentrations that meet EPA water quality standards. The WTR media had satisfactory performance for copper removal. The effluent EMCs are between 0.005 to 0.021 mg/L, and six events showed positive removal.

As the results show, the WTR-incorporated HFM plunge pool achieved good performance for TSS and P removal, which satisfied our design purpose. The WTR works as an advanced supplement material, offering a much greater phosphorus adsorption capacity than HFM to mitigate phosphorus leaching and can greatly enhance DP removal. WTR incorporation can highly improve the performance of traditional SCMs if phosphorus is the target pollutant to deal with. From an economic perspective, applying WTR in SCMs is a cost-effective approach since many drinking water treatment facilities need to pay for WTR disposal in landfills (Poor et al. 2018). It is also benefit for energy saving by reusing the WTR.

There are still some unexplored topics which might be worth studying in the future. Some research should focus on WTR which is a novel material. The phosphorus adsorption capabilities for WTR are variable if they come from different

drinking water treatment facilities. The capacities of WTR might be different even from the same treatment plant but different batches. Therefore, it is important to understand the nature of WTR and to quantify the residual phosphorus adsorption capacity before applying it into the SCMs since it is not ideal to use the phosphorus adsorption capacity quickly.

Regarding this project, future work may help us to know the lifespan of the system/WTR. Furthermore, there might be some contaminants that the WTR removed during drinking water treatment process, like lead and arsenic which have serious risk to human health (NEBRA 2019). Therefore, WTR that is to be used as a SCM supplement material should be measured for heavy metals and other potential pollutants.

In this research, composite samples were collected to evaluate the performance of the plunge pool. Composite sampling offers good estimate of the even mean concentrations and reduce the experimental analytical costs; however, temporal information cannot be collected by composite sampling. Therefore, discrete samples would be better to understand how the concentrations of pollutants changed dynamically during a single storm event.

Appendix

An example of how the $V_{Combined}$ and $V_{Baseflow}$ were determined is shown in Figure 27 to Figure 30. Figure 27 shows the precipitation (red upper section) and effluent hydrograph (black lower section) of the rainfall event recorded on December 1, 2019. The flowrate was measured and recorded every minute by the autosampler. As the hydrograph shows, there was a nearly constant baseflow from the outflow pipe detected before the rain started (left bottom corner). Since the baseflow level changes slightly, the average value was determined to represent the actual baseflow flowrate for the whole storm event ($Q_{Baseflow}$). The flowrate of the baseflow was constant during a single rainfall event, but varied with different events, ranging from 0.01-0.1 L/s. The effluent flowrate had a sudden jump after the rainfall started, which indicates that the runoff has passed through the plunge pool and arrived at the downstream pipe. The effluent flowrate changed as the rainfall continued. Then it decreased continuously and reached a constant value after the rainfall stopped for a while (because there is a lag).

To determine the total effluent volume ($V_{Combined}$), the flowrate jump point was set as the rainfall starting point, and the point where the effluent flowrate became constant (change of flowrate less than 5% within 30 minutes) after rainfall stopped was set as the ending point. $V_{Combined}$ is total area under the effluent hydrograph, which was determined from the autosampler output. The runoff duration (t) can be determined by subtracting the rainfall starting time from the ending time from

hydrograph. Then the baseflow volume ($V_{Baseflow}$) was calculated using Eq.14. The target/true effluent volume ($V_{Effluent}$) was calculated using Eq.12.

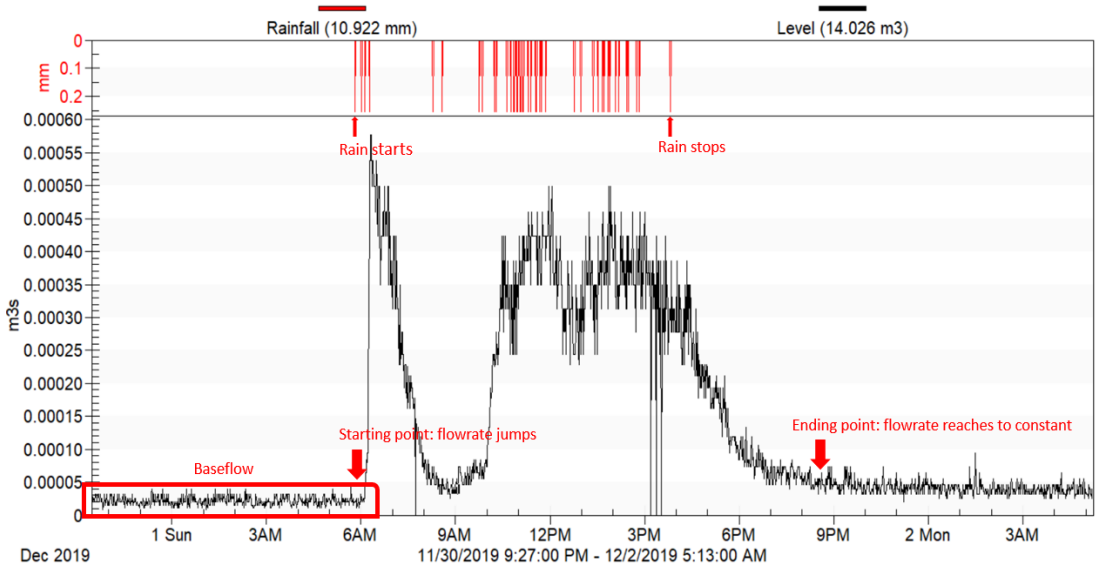

Figure 34. Precipitation and effluent hydrograph from storm event on December 1, 2019.

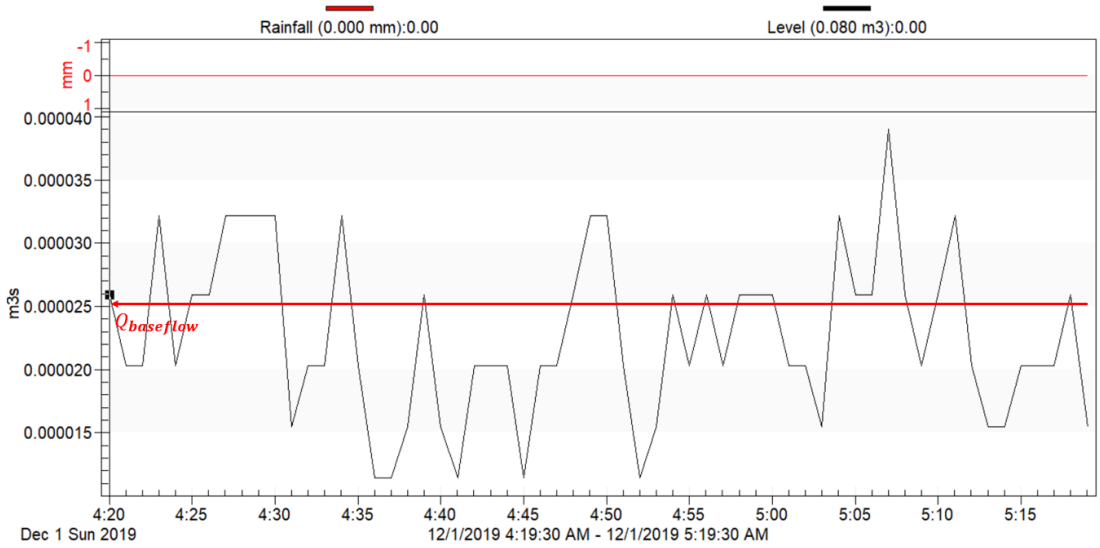

Figure 35. Zoom in the baseflow before the rain started (from left bottom corner in Figure 34).

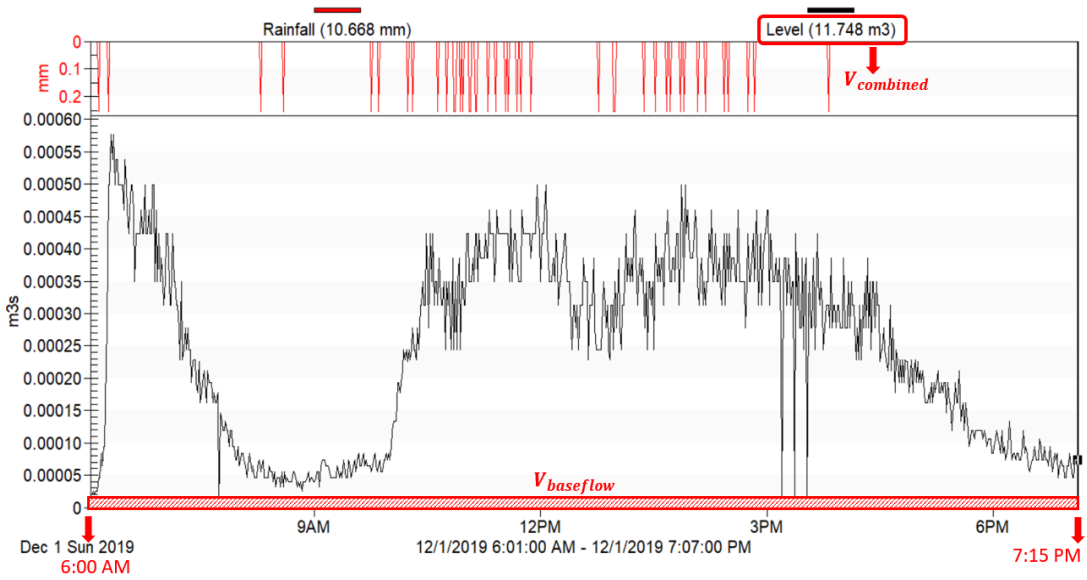

Figure 36. Interception from starting and ending points (from Figure 35).

<u>Iron Output Load</u>

C (Iron concentration): 4,143 to 7,483 ug/L (will be revised when we get more data);

T (Duration): 550 days;

Q (Baseflow Rate): 0.02 to 1.4 L/s (median = 0.065 L/s);

$$M = C * Q * T$$

M (Output Load, using 4,143 ug/L): 3,938 to 275,626 g (median = 12,797 g)

M (Output Load, using 7,483 ug/L): 7,111 to 497,829 g (median = 23,113 g)

M ranged from: 3,938 to 497,829 g (median ranged from 12,797 to 23,113 g)

<u>Iron in WTR</u>

V (volume of HFM): 0.51 m^3;

10% WTR by volume;

ρ_d (Bulk density for dry WTR) = 0.56 g/cm^3

ρ_w (Bulk density for wet WTR) = ?

w (moisture content for wet WTR) = 3.2 g wet/g dry = 2.2

m (Mass of WTR) = ?

Al content (dry) = 126,000 mg Al/kg WTR

Fe content (dry)= 10,900 mg Fe/kg WTR

M (Mass of iron) =?

$$\rho_d = \frac{\rho}{1+w}$$

$$\rho_d = dry\ density, \rho = bulk\ density$$

$$\rho_w = \rho_d * (1+w) = 0.56\ \mathrm{g}/cm^3 * (1+2.2) = 1.792\ \mathrm{g}/cm^3$$

$$m_w = \rho_w * V * 10\% = 1.792 \frac{\mathrm{g}}{cm^3} * 0.51\ m^3 * 10\% = 91.39\ kg\ wet - WTR$$

$$m_d = 91.39\ kg\ wet - WTR\ /(3.2\ \mathrm{g\ wet - WTR/g\ dry - WTR})$$

$$= 28.56\ \mathrm{g\ dry - WTR}$$

$$M = m_d * Fe\ content\ (dry) = 28.56\ kg * 10{,}900\ mg\ Fe/kg\ WTR\ = 311\ g$$

Site Photos

Figure 37. Programming upstream autosampler

Figure 38. Installing a 15-inch weir into the influent pipe

Figure 39. Installing a rain gauge

Figure 40. Connecting a battery to the autosampler

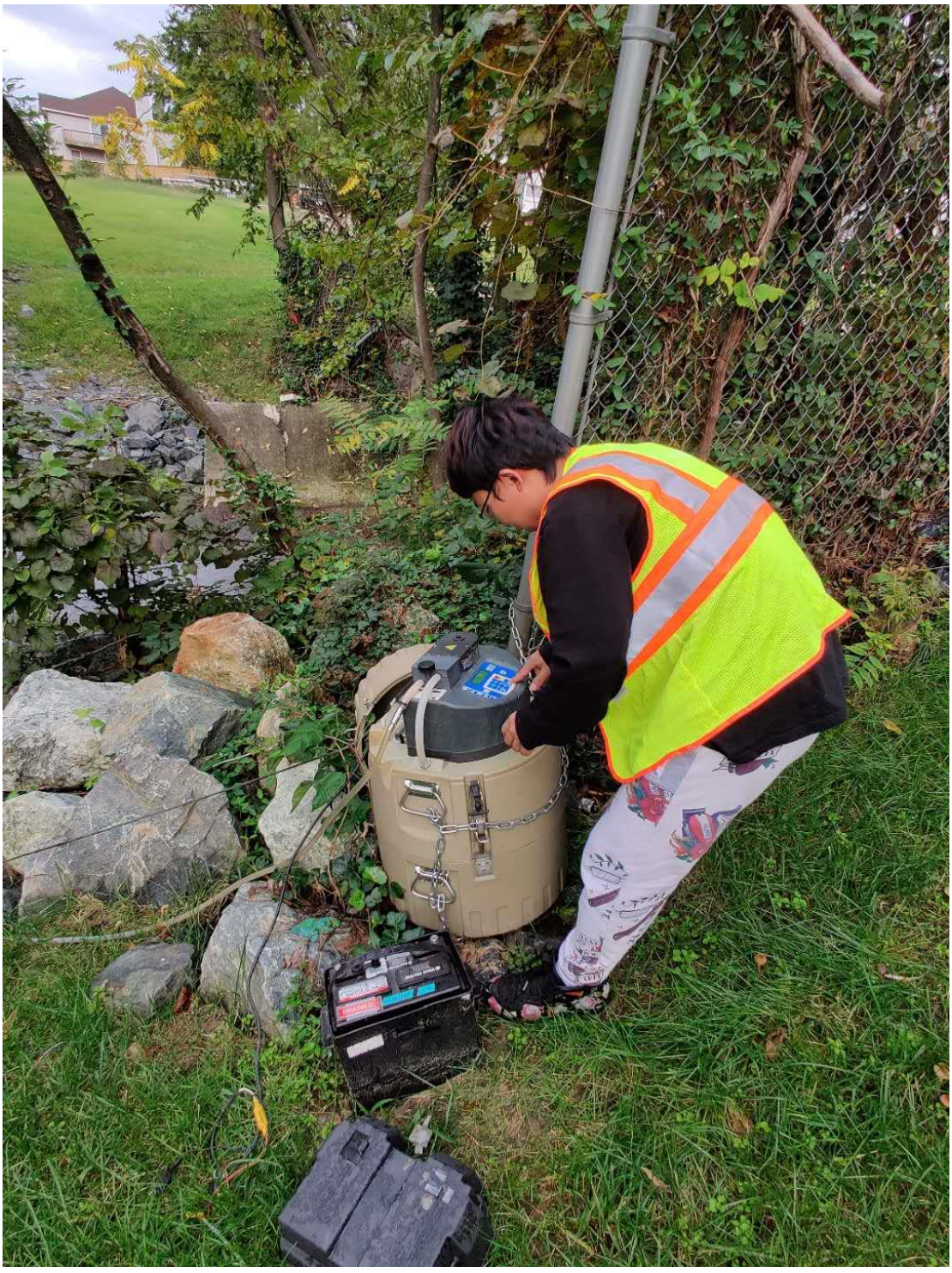

Figure 41. Programming the downstream autosampler

Figure 42. Installing a 6-inch weir into the effluent pipe

Figure 43. Collected influent samples

Figure 44. Collected effluent samples

References

American Public Health Association (APHA), American Water Works Association (AWWA), and Water Environment Federation (WEF). 2012. Standard Methods for the Examination of Water and Wastewater. American Public Health Association, Washington, D.C.

Anderson, G., and Arlidge, E. Z. 1962. The adsorption of inositol phosphates and glycerophosphate by soil clays, clay minerals and hydrated sequioxides in acid media. J. Soil Sci., 13(2), 216–224.

American Public Health Association (APHA).2005. Standard Methods for the Examination of Water and Wastewater: Centennial ed., 21 ed.; American Public Health Association.

Barrett, M. E. 2010. Evaluation of sand filter performance. Austin, TX: Univ. of Texas at Austin.

Berretta, C., and Sansalone, J. 2011. Speciation and transport of phosphorus in source area rainfall-runoff. Water, Air, Soil Pollut., 222 (1–4), 351–365.

Bohn, H., McNeal, B., O'Connor, G. A. Soil Chemistry, 2nd ed.;John Wiley and Sons: New York, 1985.

Bratières, K., Fletcher, T. D., Deletic, A., and Zinger, Y. 2008. Nutrient and sediment removal by stormwater biofilters: A large-scale design optimisation study. Water Res., 42(14), 3930–3940.

Brown, R. A., Birgand, F., and Hunt, W. F. 2013. Analysis of consecutive events for nutrient and sediment treatment in field-monitored bioretention cells. Water Air Soil Pollut., 224(6), 1–14.

Brown, T., Schueler, T., Wright, T., Winer, R., and Zielinkski, J. 2003. Maryland Chesapeake and Atlantic Coastal Bays—Critical area 10% rule guidance manual, Center for Watershed Protection, Ellicott City, MD.

Chen, S., Ling, J., and Blancheton, J.-P. 2006. Nitrification kinetics of biofilm as affected by water quality factors. Aquacult. Eng., 34 (3), 179–197.

Cho, K. W., Song, K. G., Cho, J. W., Kim, T. G., and Ahn, K. H. 2009. Removal of nitrogen by a layered soil infiltration system during intermittent storm events. Chemosphere, 76 (5), 690–696.

Cleasby, J. L., and Logsdon, G. S., Chapter 8: Granular Bed and Precoat Filtration. 1999. In Water Quality and Treatment: A Handbook of Community Water Supplies; McGraw-Hill: New York.

Collins, K. A., Lawrence, T. J., Stander, E. K., Jontos, R. J., Kaushal, S. S., Newcomer, T. A., Grimm, N. B., and Cole Ekberg, M. L. 2010. Opportunities and challenges for managing nitrogen in urban stormwater: A review and synthesis. Ecol. Eng., 36 (11), 1507–1519.

Cooke, T. D., and Bruland, K. W. 1987. Aquatic chemistry of selenium: Evidence of biomethylation. Environ. Sci. Technol., 21 (12), 1214–1219.

Davis, A. P. 2007. Field performance of bioretention: Water quality. Environ. Eng. Sci., 24 (8), 1048–1064.

Davis, A. P., and McCuen, R. H. Stormwater Management for Smart Growth; Springer Science: New York, 2005.

Davis, A. P., Shokouhian, M., Sharma, H., and Minami, C. 2006. Water quality improvement through bioretention media: nitrogen and phosphorus removal. Water Environ. Res., 78(3), 284–293.

Dayton, E.A., and Basta, N. T. 2001. Characterization of drinking water treatment residuals for use as a soil substitute. Water Environ. Res., 73 (1), 52–57.

Dietz, M., and Clausen, J. C. 2005. A field evaluation of rain garden flow and pollutant treatment. Water, Air, Soil Pollut., 167, 123–138.

Dietz, M. E., and Clausen, J. C. 2006. Saturation to improve pollutant retention in a rain garden. Environ. Sci. Technol., 40 (4), 1335–1340.

Dipankar Saha, and Asit K. Mukhopadhyay. 1981. NH_4^+ fixation by hydrated oxides of iron in soils, Communications in Soil Science and Plant Analysis, 12(1), 51–59.

Doan, L.N., and Davis, A.P. 2017. Bioretention–cistern–irrigation treatment train to minimize stormwater runoff. J. Sustain. Water Built Environ., 3, 4017003.

Erickson, A.J., Gulliver, J.S., and Weiss, P.T. 2007. Enhanced sand filtration for storm water phosphorus removal. J. Environ. Eng. 133 (5), 485–497.

Erickson, A. J., Gulliver, J. S., and Weiss, P. T. 2012. Capturing phosphates with iron enhanced sand filtration. Water Res., 46 (9), 3032–3042.

Erickson, A.J., Gulliver, J.S., and Weiss, P.T. 2017. Phosphate removal from agricultural tile drainage with iron enhanced sand. Water, 9, 672.

Genc-Fuhrman, H., Wu, P., Zhou, Y., and Ledin, A. 2008. Removal of As, Cd, Cr, Cu, Ni and Zn from polluted water using an iron based sorbent. Desalination, 226 (1–3), 357–370.

Hano, T., Takanashi, H., Hirata, M., Urano, K., and Eto, S. 1997. Removal of phosphorus from wastewater by activated alumina adsorbent. Water Sci. Technol., 35(7), 39–46.

Hatt, E., Fletcher, D., and Deletic, A. 2007. Hydraulic and pollutant removal performance of stormwater filters under variable wetting and drying regimes. Water Sci. Technol., 56 (12), 11–19.

He, J., Valeo, C., Chu, A., and Neumann, N. F. 2010. Characteristics of suspended solids, microorganisms, and chemical water quality in event-based stormwater runoff from an urban residential area. Water Environ. Res., 82 (12), 2333–2345.

Hsieh, C., and Davis, A. P. 2005. Evaluation and optimization of bioretention media for treatment of urban storm water runoff. J. Environ. Eng., 131 (11), 1521–1531.

Hsieh, C., Davis, A. P., and Needelman, B. A. 2007. Nitrogen removal from urban stormwater runoff through layered bioretention columns. Water Environ. Res., 79 (12), 2404–2411.

Hunt, W. F., Jarrett, A. R., Smith, J. T., and Sharkey, L. J. 2006. Evaluating bioretention hydrology and nutrient removal at three field sites in North Carolina. J. Irrig. Drain. Eng., 1326, 600–608.

Hunt, W. F., Smith, J. T., Jadlocki, S. J., Hathaway, J. M., and Eubanks, P. R. 2008. Pollutant removal and peak flow mitigation by a bioretention cell in urban Charlotte, NC. J. Environ. Eng., 134 (5), 403–408.

Ippolito, J. A., Barbarick, K. A., Heil, D. M., Chandler, J. P., and Redente, E. F. 2003. Phosphorus retention mechanisms of a water treatment residual. J. Environ. Qual., 32 (5), 1857–1864.

Gon Kim, J., Hyun Kim, J., Moon, H.-S., Chon, C.-M. and Sung Ahn, J. 2002. Removal capacity of water plant alum sludge for phosphorus in aqueous solutions, Chem. Speciation Bioavailability, 14, 67–73.

Kim, H., Seagren, E. A., and Davis, A. P. 2003. Engineered bioretention for removal of nitrate from stormwater runoff. Water Environ. Res., 75 (4), 355–367.

Kreeb, L. B. 2003. Hydrologic efficiency and design sensitivity of bioretention facilities. Honors Research thesis, Dept. of Civil and Environmental Engineering, Univ. of Maryland.

Landsman, M. R., and Davis, A. P. 2018. Evaluation of nutrients and suspended solids removal by stormwater control measures using high-flow media. J. Environ. Eng., 144(10), 04018106.

Lei, L., and Davis, A.P. 2019. (Unpublished data).

Li, H., and Davis, A. P. 2009. Water quality improvement through reductions of pollutant loads using bioretention. J. Environ. Eng., 135 (8), 567–576.

Li, H., and Davis, A. P. 2008. Urban particle capture in bioretention media. I: Laboratory and field studies. J. Environ. Eng., 134 (6), 409–418.

Li, H., and Davis, A. P. 2008. Urban particle capture in bioretention media. II: Theory and model development. J. Environ. Eng., 134 (6), 419–432.

Li, H., and Davis, A. P. 2008. Heavy metal capture and accumulation in bioretention media. Environ. Sci. Technol., 42 (14), 5247–5253.

Li, L., and A. P. Davis. 2014. Urban stormwater runoff nitrogen composition and fate in bioretention systems. Environ. Sci. Technol., 48 (6), 3403–3410.

Liu, J., and A. P. Davis. 2013. Phosphorus speciation and treatment using enhanced phosphorus removal bioretention. Environ. Sci. Technol., 48 (1), 607–614.

Local Weather Forecast, News and Conditions. (n.d.). Retrieved April 20, 2020, from https://www.wunderground.com/

Lucas, W. C., and Greenway, M. 2008. Nutrient retention in vegetated and nonvegetated bioretention mesocosms. J. Irrig. Drain. Eng., 134 (5), 613–623.

Lucas, W. C., and Greenway, M. Phosphorus retention by bioretention mesocosms using media formulated for phosphorus sorption: Response to accelerated loads. J. Irrig. Drain. Eng., 2011, 137 (3), 144–153.

Namasivayam, C., and Ranganathan, K. 1995. Removal of Pb(II), Cd(II), Ni(II) and mixture of metal-ions by adsorption onto waste Fe(III)/Cr(III) hydroxide and fixed-bed studies. Environmental Technology, 16 (9), 851–860.

Natarajan, P., and Davis, A. P. 2016. Performance of a ‘transitioned’ infiltration basin. 2: Nitrogen and phosphorus removals. Water Environ. Res., 88(4), 291–302.

NEBRA. (n.d.). Retrieved April 20, 2020, from https://www.nebiosolids.org/

NRCS (Natural Resources Conservation Service). 1986. Urban hydrology for small watersheds. NRCS TR-55. Washington, DC: NRCS.

O’Neill, S. W., and Davis, A. P. 2012. Water treatment residual as a bioretention amendment for phosphorus. II. Long-term column studies. J. Environ. Eng., 138 (3), 328–336.

Ostrom, T.K., Aydilek, A.H., and Davis, A.P. 2019. High-flow structural media for removing stormwater-dissolved phosphorous in permeable paving. J. Sustain. Water Built Environ., 5 (2), 04019001.

Ostrom, T. K., and Davis, A. P. 2019. Evaluation of an enhanced treatment media and permeable pavement base to remove stormwater nitrogen, phosphorus, and metals under simulated rainfall. Water Res., 166, 115071.

Parfitt, R. L., Russell, J. D., and Farmer, V. C. 1976. Confirmation of the surface structures of goethite (α-FeOOH) and phosphated goethite by infrared spectroscopy. J. Chem. Soc.: Faraday Trans., 72, 1082–1087.

Passeport, E., Hunt, W. F., Line, D. E., Smith, R. A., and Brown, R. A. 2009. Field study of the ability of two grassed bioretention cells to reduce storm-water runoff pollution. J. Irrig. Drain. Eng., 135 (4), 505–510

Pitt, R., Maestre, A., Morquecho, R., Brown, T., Schueler, T., Cappiella, K., and Sturm, P. 2005. Evaluation of NPDES Phase 1 Municipal Stormwater Monitoring Data. University of Alabama and the Center for Watershed Protection.

Poor, C. J., Conkle, K., Macdonald, A., and Duncan, K. 2019. Water treatment residuals in bioretention planters to reduce phosphorus levels in stormwater. Environmental Engineering Science, 36(3), 265–272.

Qiu, F., Zhao, S., Zhao, D., Wang, J., and Fu, K. 2019. Enhanced nutrient removal in bioretention systems modified with water treatment residuals and internal water storage zone. Environ. Sci. Water Res. Technol., 5, 993–1003.

Reddy, K. R., and D'Angelo, E. M. 1994. Soil processes regulating water quality in wetlands. Global wetlands: Old world and new, W. J. Mitsch, ed., Elsevier, New York, 309–324.

Shang, C., Huang, P. M., and Stewart, J. W. B. 1990. Kinetics of adsorption of organic and inorganic phosphates by short-range ordered precipitate of aluminum. Can. J. Soil Sci., 70(3), 461–470.

Shang, C., Stewart, J. W. B., and Huang, P. M. 1992. pH effects on kinetics of adsorption of organic and inorganic phosphates by short-range ordered aluminum and iron precipitates. Geoderma, 53(1–2), 1–14.

Shumilovskikh, L. S., Schlütz, F., Achterberg, I., Kvitkina, A., Bauerochse, A., and Leuschner, H. H. 2015. Pollen as nutrient source in Holocene ombrotrophic bogs. Rev. Palaeobot. Palynol., 221(15), 171–178.

Stumm, W., and Morgan, J.J. 1981. Aquatic Chemistry: An Introduction Emphasizing Chemical Equilibria in Natural Waters, 2nd ed.; Wiley: New York, NY, USA, p. 780

Taylor, G. D., T. D. Fletcher, T. H. F. Wong, P. F. Breen, and H. P. Duncan. 2005. Nitrogen composition in urban runoff—Implications for stormwater management. Water Res., 39 (10), 1982–1989.

United States Environmental Protection Agency (USEPA). 1986. Quality Criteria for Water. United States Environmental Protection Agency, Office of Water, Washington, D.C.

United States Environmental Protection Agency (USEPA). 1988. Ambient Water Quality Criteria for Aluminum. United States Environmental Protection Agency, Office of Water, Washington, D.C.

United States Environmental Protection Agency (USEPA). 1996. Water Quality Criteria Documents for the Protection of Aquatic Life in Ambient Water. United States Environmental Protection Agency, Office of Water, Washington, D.C.

United States Environmental Protection Agency (USEPA). 1999. Preliminary data summary of urban storm water best management practices. EPA-821-R-99-012, Washington, D.C.

United States Environmental Protection Agency (USEPA). 2000. Ambient Water Quality Criteria Recommendations. United States Environmental Protection Agency, Office of Water, Washington, D.C.

United States Environmental Protection Agency (USEPA). 2016. Draft Aquatic Life Ambient Estuarine/Marine Water Quality Criteria for Copper. United States Environmental Protection Agency, Office of Water, Washington, D.C.

Urbonas, B. R. 1999. Design of a sand filter for stormwater quality enhancement. Water Environ. Res., 71 (1), 102–113.

Water Environment Federation and ASCE WEF/ASCE. 1998. Urban runoff quality management. WEF Manual of Practice No. 23, ASCE Manual and Rep. on Engineering Practice No 87, WEF, Alexandria, Va., ASCE, Reston, Va.

Wu, P., and Zhou, Y. 2009. Simultaneous removal of coexistent heavy metals from simulated urban stormwater using four sorbents: a porous iron sorbent and its mixtures with zeolite and crystal gravel. J. Hazard. Mater., 168 (2–3), 674–680.

Yan, Q., Davis, A. P., and James, B. R. 2016. Enhanced organic phosphorus sorption from urban stormwater using modified bioretention media: Batch studies. J. Environ. Eng., 142 (4), 04016001.

Yao, K.-M., Habibian, M. T., and O'Melia, C. R. 1971. Water and wastewater filtration. Concepts and applications. Environ. Sci. Technol., 5 (11), 1105–1112.

He, Z. L., Alva, A. K., Li, Y. C., Calvert, D. V., and Banks, D. J. 1999. Sorption-desorption and solution concentration of phosphorus in a fertilized sandy soil, J. Environ. Qual., 28, 1804

Zinger, Y., Blecken, G. T., Fletcher, T. D., Viklander, M., and Deletic, A. 2013. "Optimising nitrogen removal in existing stormwater biofilters: Benefits and tradeoffs of a retrofitted saturated zone." Ecol. Eng., 51, 75–82.